FEDERAL UNIVERSITY OF ESPÍRITO SANTO
DEPARTMENT OF ENVIRONMENTAL ENGINEERING
ENVIRONMENTAL ENGINEERING POSTGRADUATE PROGRAM

IMPACT ASSESSMENT ON THE HYDRODYNAMICS OF THE SAN QUINTIN BAY LAGOON, BAJA CALIFORNIA - MEXICO: DEEPENING A NORTHEAST REGION.

by

MARIA FERNANDA MORALES SANTILLÁN

Vitória
2020

MARIA FERNANDA MORALES SANTILLÁN

IMPACT ASSESSMENT ON THE HYDRODYNAMICS OF THE SAN QUINTIN BAY LAGOON, BAJA CALIFORNIA - MEXICO: DEEPENING A NORTHEAST REGION.

Dissertation submitted in partial fulfillment of the requirements for the degree of Master of Environmental Engineering in the Environmental Engineering Graduate Program, Federal University of Espírito Santo.

Advisor: Prof. Dr. Julio Tomás Aquije Chacaltana

Co- Advisor: Dr. Adán Mejía Trejo

Financial support: CAPES

Institutional support: LABESUL (UFES)

Vitória

2020

MARIA FERNANDA MORALES SANTILLÁN

IMPACT ASSESSMENT ON THE HYDRODYNAMICS OF THE SAN QUINTIN BAY LAGOON, BAJA CALIFORNIA - MEXICO: DEEPENING A NORTHEAST REGION.

Dissertação apresentada ao Programa de Pós-Graduação em Engenharia Ambiental do Centro Tecnológico da Universidade Federal do Espírito Santo, como requisito parcial para obtenção do Grau de Mestre em Ciências em Engenharia Ambiental na Área de Concentração Recursos Hídricos.

Aprovada 28 em fevereiro de 2020.

COMISSÃO EXAMINADORA

_____

Prof. Dr. Julio Tomás Aquije Chacaltana
Universidade Federal do Espírito Santo
Orientador

_____

Prof. Dr. Adán Mejía Trejo
Universidad Autónoma de Baja California
Co - Orientador

_____

Prof. Dr. José Antonio Tosta dos Reis
Universidade Federal do Espírito Santo
Examinador Interno

_____

Prof. Dr. Marcos Nicolas Gallo
Universidade Federal de Rio de Janeiro
Examinador Externo

ACKNOWLEDGMENTS

Agradezco primeramente a Dios y a la vida por haber tenido la oportunidad de realizar mis estudios de maestría con el soporte de personas increíbles.

Quiero agradecer especialmente al Dr. Julio Aquije Chacaltana por haberme recibido en su grupo de investigadores, por apoyarme durante estos dos años, por enseñarme tanto, pero sobre todo, por enseñarme a retarme a mí misma.

Al Dr. Adán Mejía Trejo, por el apoyo en los datos para la realización de éste trabajo, por su guía, y sobre todo por su confianza en mí.

A la CAPES por el auxilio financiero.

A mis amigos de LABESUL, Kaio, Fran, Leo, Fabio, Gaby, Mirela, Matheus, Luana y Gregorio, mil gracias por su compañía, por su apoyo, por las risas y por haberme ayudado en tanto.

A la familia brasileña que me acompañó desde mi llegada: Ricardo, Richito, Mayra, Emerson, Mary, Alessandra, Roberto, y sobre todo, Brendo, mil gracias por hacer cada desayuno un momento para conversar sobre la vida, sobre sueños, etc.

Quiero hacer un agradecimiento muy especial a Sadi, porque sin ti la vida hubiera sido simplemente sin colores. Gracias por escogerme tu a mí y por salvarme de tantas noches de soledad y tristeza.

A Daniel, porque aunque no lo sepas, fuiste un salvavidas gigante para mí en estos meses, gracias por tantas horas de pláticas desde el otro lado del mundo.

A Nereo, porque fuiste el impulso para atreverme a ir por más.

Finalmente quiero agradecer a las personas más importantes en mi vida, y sin quienes este viaje jamás hubiera sido posible, mis padres y mi hermana, Reno, a quienes dedico este trabajo y a quienes he extrañado cada día. Agradezco infinitamente su amor, paciencia, cariño, y el jamás dejarme desistir en el proceso. Gracias por hacerme la persona que soy, por apoyarme en cada decisión y en cada locura, aunque nunca sepamos como va a terminar. Infinitas gracias por creer en mi cuando yo no lo hice.

“Caminante no hay camino,
Se hace camino al andar.
Al andar se hace camino
Y al volver la vista atrás
Se ve la senda que nunca se ha de volver a pisar…”

Juan Manuel Serrat

ABSTRACT

Commonly, coastal water bodies are subject to anthropic action due to the various human activities that take place near the coast. Any change in the coastline or coastal sea bed directly impacts the behavior of the local water movement. It is extremely important to know the scope of the environmental impact, whether they are limited to the place of human intervention or if they spread far from it. In the latter case, it is a priority to know quantitatively the order of magnitude of the impact caused to the environment in order to evaluate the mitigation measures to obtain the much-desired sustainable development. It is well known that the impact on the aquatic environment has the potential to cause changes in hydrodynamics, which in turn causes changes in sediment transport, which can change navigation capacity, water quality and coastal flood patterns. This work investigates changes in hydrodynamics due to the deepening of a seabed region of a coastal water body. With the purpose of boosting tourism in the coastal lagoon of Bay of San Quintín Lagoon (SQBL), in 2014 a dredging project was proposed in the north of the east branch of the Lagoon of the Bay of San Quintín. This coastal lagoon is a body of hypersaline water formed by two arms (east and west) and it is located north of Mexico in the Pacific Ocean. The project intends to change the depth from 0.5 m to 2 m in an area of 116,221 m^2. In order to understand the impact of deepening on hydrodynamics, this work has used the computational fluid mechanics technique, in this sense and for the purposes of this work, Delft3D was used. The model was set up in the study region and the astronomical tide and the wind were the external forces considered to force the model. Numerical simulations were performed to assess the sensitivity of the hydrodynamic model. To assess the influence of the deepening on hydrodynamics, two scenarios were considered, without and with a deepening region. Results are presented for the spatial and temporal behavior of both water level and water velocity. The comparison of numerical results with those measured in the field showed a good performance, with errors of 4% in elevation and 12% averaged in currents. The results during the simulation period showed that in the deepened region there was a maximum reduction in the tide height during the spring tide, reaching maximum values of 0.47 m while changes in the tide height during low tide was imperceptible. On average, in the simulated

period, there was a decrease of 4 cm in the water level with deepening. Regarding the water velocity, the greatest variations also occur during the spring tides. A maximum reduction of 0.14 m/s was found in the deepening region, representing a decrease in speed of approximately 70% when compared to the velocity without deepening. Finally, the results suggest that the deepening of the study area causes a localized impact, generally producing a decrease in the magnitudes of the flow velocity over the deepened region.

Key words: hydrodynamic modelling, deepening, Delft3D

RESUMO

Geralmente, os corpos d'água costeiros estão sujeitos a ação antrópica devido às várias atividades humanas que ocorrem perto da costa. Qualquer mudança no contorno da costa ou no fundo do mar afeta diretamente o comportamento do movimento local da água. É extremamente importante conhecer o alcance do impacto ambiental, se ele está limitado ao local da intervenção humana ou se ele se espalha para longe. Neste último caso, é prioritário conhecer quantitativamente a ordem de magnitude do impacto causado ao meio ambiente, a fim de avaliar as medidas de mitigação para obter o tão desejado desenvolvimento sustentável. É sabido que o impacto no ambiente aquático tem o potencial de causar mudanças na hidrodinâmica, que, por sua vez, causa mudanças no transporte de sedimentos, o que pode alterar a capacidade de navegação, a qualidade da água e os padrões de inundação costeira. Este trabalho investiga mudanças na hidrodinâmica devido a atividade de aprofundamento de uma região noroeste de um corpo de água costeiro. Com o objetivo de impulsionar o turismo na lagoa costeira da Lagoa da Baía de San Quintín (SQBL), em 2014, um projeto de dragagem foi proposto no norte do ramo leste da Lagoa. Esta lagoa costeira é um corpo de água hipersalina formada por dois braços (leste e oeste) e está localizada ao norte do México no Oceano Pacífico. O projeto pretende alterar a profundidade de 0,5 m a 2 m em uma área de 116.221 m2. Para entender o impacto do aprofundamento na hidrodinâmica, este trabalho utilizou a técnica da mecânica dos fluidos computacional; nesse sentido e para os fins deste trabalho, foi utilizado o Delft3D. O modelo foi implementado na região de estudo e a maré astronômica e o vento foram as forçantes externas consideradas para o modelo. Simulações numéricas foram realizadas para avaliar a sensibilidade do modelo hidrodinâmico. Para avaliar a influência do aprofundamento na hidrodinâmica, foram considerados dois cenários, sem e com a região de aprofundamento. Os resultados são apresentados para o comportamento espacial e temporal do nível e velocidade da água. A comparação dos resultados numéricos com os medidos em campo mostrou um bom desempenho, com erros de 4% em elevação e 12% em média em correntes. Os resultados durante o período de simulação mostraram que na região aprofundada houve uma redução máxima da altura da maré durante a maré de sizígia, atingindo valores máximos de 0,47 m, enquanto as mudanças

na altura da maré durante a maré de quadratura eram imperceptíveis. Em média, no período simulado, houve uma diminuição de 4 cm no nível da água com o aprofundamento. Em relação à velocidade da água, as maiores variações também ocorrem durante as marés de sizígia. Foi encontrada uma redução máxima de 0,14 m/s na região de aprofundamento, representando uma diminuição na velocidade de aproximadamente 70% quando comparada à velocidade sem aprofundamento. Finalmente, os resultados sugerem que o aprofundamento da área de estudo causa um impacto localizado, geralmente produzindo uma diminuição nas magnitudes da velocidade do escoamento sobre a região aprofundada.

Palavras-chave: modelagem hidrodinâmica, aprofundamento, Delft3D

LIST OF FIGURES

LIST OF TABLES

SUMMARY

1. INTRODUCTION

Coastal systems are among the most dynamic physical systems on earth and are subject to a large variety of forces. Estuaries and coastal lagoons are systems with a high primary production; these include a high diversity and density of fish and invertebrates, so they are important at the global level both from an ecological and economic point of view (HOSACK et al., 2006).

In coastal lagoons (hypersaline ones), tides are the most important factor in their hydrodynamics. For this reason and because they are generally very shallow, they tend to be vertically homogeneous. However, the wind, the solar radiation, and the high atmospheric temperature of the latitudes in which they are predominantly found, produce evaporation in the extensive superficial zones near the head, sufficient to originate a longitudinal salinity gradient increasing towards the head.

A vertical gradient appears, increasing towards the surface and heating in these same zones, originating a longitudinal gradient of temperature increasing towards the head (FARRERAS , 2006).

Coastal lagoons frequently present human settlements, which commonly translate into alterations inside and outside this water bodies. These man-made alterations, talking specifically on those ones inside the lagoons, modify the tidal exchange in coastal embayment's, disrupting the pathway of the tidal waters entering and the tidal range and flushing characteristics of these systems.

In Mexico, coastal lagoons have great socioeconomic importance, since they are the seat of food, energy, tourism, housing and communication resources, and it is urgent to take advantage of and develop harmoniously, simultaneously preserving the natural environment (balance between exploitation and preservation) (FARRERAS , 2006). Rapid population and tourism growth, as well as the aquaculture and agriculture activities that have developed around these water bodies can cause negative environmental impacts in these ecosystems.

The San Quintín Bay Lagoon (SQBL) is a coastal lagoon located in the North Pacific Mexican State of Baja California between 30 ° 24 'and 30 ° 30' north latitude and 115 ° 57 'and 116 ° 01' west longitude. This lagoon is divided by two arms named San Quintin Bay (SQB) and False Bay (FB). This sequestered spot is recognized worldwide for its biodiversity and its hemispheric importance to fisheries, waterflow, migratory birds and other coastal resources (ALCAZAR et al., 2016).

This lagoon is one of the most important coastal lagoons at the Pacific of Baja California that is characterized by its high capacity of aquaculture and agricultural production (CASIAN, 1996). Currently, the Japanese oyster farming (Crassostrea gigas) represents the most important economic resource of fishermen in the region (MONREAL; DE LEÓN, 1990); therefore, for the aquaculture sector, it is a priority to maintain a good quality of water, especially the sanitary status of it, which in Mexico is regulated by the Ministry of Public Health.

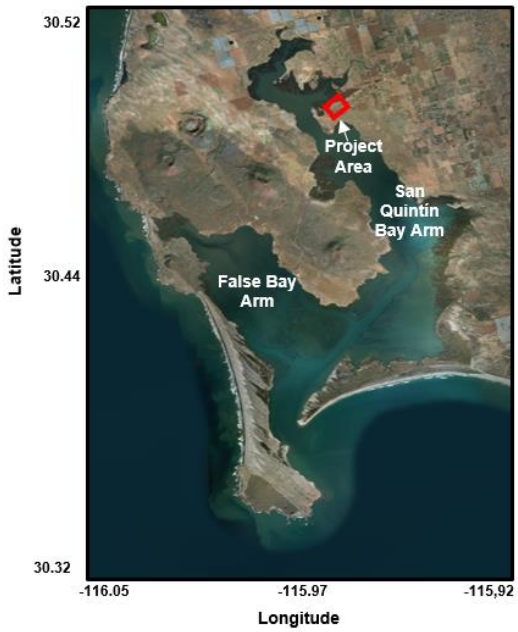

Figure 1. San Quintin Bay Lagoon. The project area is marked in a red square.

On May 23, 2014, the Environmental Ministry of Mexico received a project, in which the main objective was the construction of a dock in the north area of the eastern arm (SQB). This report projected a dredging activity, removing material from an area of 116,221 m^2 and expected to dredge a volume of 2,752.75m^3, this in order to modify the bathymetry from 0.5 m to 2 m depth (Figure 1).

The proposed project has the potential to cause changes in hydrodynamics and sediment transport, usually responsible for changes, positive or negative, in water quality, erosion, sedimentation, navigation capacity and coastal flood patterns (LACERDA, 2016). These effects are evident at remarkable sites such as the Ems estuary (VAN MAREN et al., 2015) and the San Francisco Bay (KNOWLES; CAYAN, 2004).

The deepening of estuaries, lagoons, bays, etc. in dredging projects, even within a few meters (~ 2-3 m), can result in impacts that alter the patterns, currents, and salinity gradients. Among these possible impacts and their consequences (ABBOTT; PRICE, 1994) highlights: i) Increased tidal inflow, resulting in higher pre-loading upstream of the estuary/river, increasing flood risk; ii) increased tidal inflow, resulting in intensification of low tides and deepening of the channel due to erosion of the bottom; iii) intensification of flood currents and ebb, resulting in higher concentrations of suspended sediment (SSC); iv) intensification of saltwater inflow, resulting in the reallocation of existing preferential deposition zones; and v) creating a new and/or increased demand for maintenance dredging.

The environmental impact that is generated on the coastal lagoons requires, first and foremost, the knowledge of the hydrodynamics of the system, that is, knowing how the water is moving, to which agents its movement is due, which of these could be controlled, and how will move to any possible natural or artificial modifications.

Mathematical models can be used to understand and describe processes that affects the coastal lagoon hydrodynamics and major ecological components. They can also be used to predict the response of the system under given conditions or constraints by replicating the physical behavior of a system on a computer.

There are different numerical models used to represent the hydrodynamics of a system, depending on the phenomena that you wish to simulate. Among them is

Delft3D for hydrodynamics, water quality, waves, sedimentation, etc., ADCIRC for coastal circulation, D-WAVE, SWAN, STWAVE, RCPWAVE for waves and ELCOM-CAEDYM, RMA2-RMA4 for water quality (MAZCOSTA, 2018).

Delft3D-FLOW is a multidimensional hydrodynamic (2D or 3D) simulation tool that calculates non-steady flow and transport phenomena resulting from tidal and meteorological forcing on a curvilinear, boundary-fitted grid (DELTARES, 2014). Delft3D solves nonlinear equations in shallow water. Shallow water equations (SWE) are obtained by averaging the Navier-Stokes equation in the vertical direction.

To understand the behavior of the San Quintin Bay Lagoon (BSQL) and how the human activity can impact it, a numerical model can be implemented. Numerical modelling is a methodology of great potential for studies of this character, since the implementation of a numerical model is a way of validating the hypotheses that are raised about the potential impacts resulting from these interventions (WINTERWERP et al., 2013).

To date, the use of numerical models for the description of BSQL hydrodynamics is limited to hydrodynamic models of one dimension (LUCERO, 1979; GOMEZ, 1980; TORRES, 1980) and two-dimensional models (HERNANDEZ, 2005). The work with 3D models has focused on the description of specific processes such as the validation and calibration of speeds and changes in sea level (RAMIREZ , et al., 2014), and the influence of eddies and mixing processes in the region of the mouth (JUAREZ, 2014), both by means of the Delft3D model.

Due to the lack of studies on analyzing and predicting the future impacts in hydrodynamics through human planned interventions, specifically deepening by dredging activity, this research work intends, using the principles of the fluid mechanics, to generate a computational study of the hydrodynamics that govern the SQBL through a 2D numerical model, using the open source software Delft3D.

2. OBJECTIVES

2.1 General

- Assess the changes introduced in the water body when deepening the north area of one of the arms of the coastal lagoon San Quintín Bay Lagoon (SQBL), located in Baja California, Mexico.

2.2 Specific

- To apply Computational Fluid Mechanics to determine the movement of water in the San Quintín Bay Lagoon.
- To define a strategy to address the influence of the deepening of the north area of the eastern arm of the coastal lagoon of the San Quintín Bay Lagoon.
- To quantify the impact of deepening the north of the east arm of the San Quintín Bay Lagoon on the local hydrodynamics.

3. BIBLIOGRAPHIC REVIEW

3.1.1. General dynamics

The movements of water above the solid and porous surface of the Earth, such as oceans, rivers, lagoons, etc., obey physical conservation laws that are mathematically represented by the continuity and Navier-Stokes equations. In shallow bodies of water, these equations can be treated in a particular way to propagate long waves. Waves whose wavelengths are much greater than the depth of the water and which have some special properties (PUGH, 1987).

Long waves propagates at a speed governed by depth, $(gh)^{1/2}$, so any long wave of any wavelength propagates with the same speed at a given depth (h). So, in a shallow body of water, bathymetry is essential for a correct representation of the wave transformations during its propagation in the aquatic environment. Also, moving water particles are affected by the rotation of the earth, this effect of rotation is represented by the Coriolis forces that must be included in the equation of motion.

In shallow water the amplitudes of the waves become a significant fraction of the total water depth. In addition, the stronger currents which develop in the shallow water are resisted by the drag due to bottom friction, a process which eventually removes much of the propagating tidal energy, and reduces the wave amplitudes. A further distorting factor is the influence of topography. Irregular coastlines and varying depths impose complicated tidal current patterns; where currents take curved paths, there must be associated surface gradients to provide the necessary cross-stream accelerations (PUGH, 1987).

3.1.2. Coastal lagoon dynamics

Lankford (1976), defined a coastal lagoon as a depression in the coastal zone, below the mean higher high water (MHHW), which has a permanent or ephemeral connection with the sea, but protected from it by some type of bar. Coastal lagoon hydrodynamics are mainly influenced by tides and winds as well as the lagoon

internal configuration (FISCHER, 1972).

In non-estuarine coastal lagoons, due to the absence of significant contribution of freshwater from rivers, tides are the most important factor in their dynamics. Because for the above, and because the reason between the discharge of the river and the discharge of the tide is very small or zero, and the width greater than 20 times the depth (they are generally very shallow), this water bodies tend to be vertically homogeneous. However, wind, solar radiation, and the high atmospheric temperature of the latitudes in which they are predominantly found, produce:

- Evaporation in the large surface areas near the head, enough to cause a longitudinal salinity gradient increasing towards the head, and another vertical one increasing towards the surface.
- Heating in these same areas, causing a longitudinal temperature gradient also increasing towards the head, and another vertical one also increasing towards the surface (FARRERAS, 2006).

The vertical density gradient is another important factor in the exchange of water between a coastal lagoon and the adjacent ocean. The saltier and denser water is transported along the bottom towards the ocean, while the less salty and lighter water makes it into the lagoon near the surface. This two-layer circulation not only transports salt, but also heat and other chemical or organic properties of water (BAKUN; NELSON, 1977).

Coastal upwelling indirectly affects any body of water adjacent to the coast, say coastal lagoons, estuaries or bays. In coastal bodies where the dynamics are controlled by tidal currents, exchanges arise because the spatial distribution of currents and transported properties is not symmetric (STOMMEL; FORMER, 1952).

For periods of the predominant components of the tide, (Ex. $T \approx 12.4$ hours for the semidiurnal) and the typical vertical tidal ranges in most of the coastal lagoons (Ex. 2.5 m), the vertical travel speeds of the Water-free surface (approx. $1.1 \times 10^{-}$

^{4} m / s in this example) is 10^{-3} to 10^{-4} times lower than the horizontal velocities of the particles (currents) so they are neglected, considering only the horizontal components of speed in propagation.

3.2. Numerical and mathematical models

Numerical ocean models have proven to be essential for the creation of forecast estimates, as well as weather forecasts for coastal areas. Water quality studies that require an understanding of the processes that occur in the water body require a greater scope of spatial-temporal analysis to demonstrate cause and effect relationships, and numerical models are important tools for such analysis (ENTRINGER, 2016).

The complexity of the natural surface water environment combined with the ever increasing capabilities of computers to simulate the temporal evolution of systems represented by differential equations has made hydrodynamic and water quality models essential tools for both science and management (GANG JI, 2008).

Over the past few years, hydrodynamic modelling of lakes, lagoons and rivers has become an important tool for managing water resources, especially in modelling the dispersion of pollutants and morphological analysis. For example, (FERRARIN et al., 2008) designed a model to simulate the hydrodynamics and the morphology of Lake Venice, in Italy; Siqueira et al. (2007) described a three-dimensional Computational Fluid Dynamics model to simulate the dispersion of effluents in rivers; Gobbi et al. (2003), implemented a hydrodynamic and water quality model for the Lake Irai, in the metropolitan region of Curitiba, Brazil; Vargas et al. (2003) studied water circulation and pollutants dispersion in the south lakes complex of Santa Catarina State, Brazil.

Siqueira et al. (2007), described mathematical modelling as the description of physical phenomena through mathematical equations (Partial Differential Equations - PDEs). In the case of coastal regions, the main physical phenomenon studied is the hydrodynamic circulation, which is a physical process affected by

several dynamic agents such as: wind, tide, region geometry, background roughness, vegetation, among others. However, it is important to note that due to the great complexity of describing these physical phenomena, the analytical solution of these PDEs is almost always not viable. Therefore, the use of numerical solutions is preferable in view of the advantages offered.

A variety of models has been developed, and most of this model were developed by finite difference methods. This method consists of an approximation of partial derivatives by algebraic expressions with the values of the dependent variable in a limited number of selected points. As a result of the approximation, the partial differential equation that describes the problem is replaced by a finite number of algebraic equations, in terms of the values of the dependent variable at selected points.

Several open source codes (Delft3D, ADCIRC, TELEMAC, among others) have been developed recently for modelling coastal hydrodynamics and coastal processes in general.

There are different numerical models used to represent the hydrodynamics of a system, depending on the phenomenon that you wish to simulate. A lot of different criteria can be used to decide which model to use for a particular situation based on some important factors (FITZPATRICK; IMHOFF, 2001), among them is ADCIRC for coastal circulation, D-WAVE, SWAN, STWAVE, RCPWAVE for waves and ELCOM-CAEDYM, DELFLOW-DELWAQ, RMA2-RMA4 for water quality (MAZCOSTA, 2018).

In specific, the numerical model Delft3D have been applied to study a wide range of sites and phenomena.

3.2.1 Hydrodynamic model Delft3D

The Delft3D is an open source software, which consists of various modules that are used to model the particular physics of the water system, such as the

hydrodynamics, morphology and water quality. Delft3D allows to simulate the interaction of water, sediment, ecology and water quality in time and space. It is mostly used for the modelling of natural environments like coastal, river and estuarine areas, but it is equally suitable for more artificial environments like harbours, locks, etc.

Delft3D available modules are D-FLOW, D-MORPHOLOGY, D-WAVES, D-WATER QUALITY, D-ECOLOGY, D-PARTICLE TRACKING. The Delft3D-FLOW is a multi-dimensional (2D or 3D) hydrodynamic (and transport) simulation program which calculates non-steady flow and transport phenomena that result from tidal and meteorological forcing on a rectilinear or a curvilinear, boundary fitted grid (DELTARES, 2014).

The hydrodynamic conditions (velocities, water elevations, density, salinity, vertical eddy viscosity and vertical eddy diffusivity) calculated in the Delft3D-FLOW module are used as input to the other modules of Delft3D (FLANDERS MARINE INSTITUTE, 2016).

In Delft3D-FLOW the horizontal physical model domain (x,y) is covered with a curvilinear orthogonal grid, designed and optimized for a given application through a grid generator (in Cartesian or spherical co-ordinates). The horizontal resolution of the grid depends on the characteristic length scale of the bathymetry and the land-water boundary and of flow patterns that want to be resolved (DELTARES, 2014).

Modelling of the hydrodynamics and water quality in these areas requires accurate treatment of the vertical exchange processes. The accuracy of the discretization of the vertical exchange processes is determined by the vertical grid system. The two commonly used vertical grid systems in shallow-water models are the z-coordinate system (Z-model) and the so-called σ-coordinate system (σ -model) (GERRISTEN et al., 2007).

The computational model solves the three-dimensional Navier-Stokes and transport differential equations (under the shallow-water and Boussinesq

assumptions), discretizing them into finite differences and a code written in FORTRAN language.

In the shallow water the characteristic depth d is much smaller than the horizontal scale of motions L:

$$\delta = \frac{d}{L} \ll 1 \qquad 1$$

The equations of the three-dimensional hydrostatic shallow water are shown in rectangular cartesian coordinates in the horizontal (ξ, η) and in σ coordinates for the vertical. These equations express the physical principle of mass and momentum conservation (GERRITSEN et al., 2007):

$$\frac{\partial u}{\partial t} + u\frac{\partial u}{\partial x} + v\frac{\partial u}{\partial y} + \frac{\omega}{d+\zeta}\frac{\partial u}{\partial \sigma} - fv = -\frac{1}{\rho}P_u + F_u + \frac{1}{(d+\zeta)^2}\frac{\partial}{\partial \sigma}(V_v\frac{\partial u}{\partial \sigma}) \qquad 2$$

$$\frac{\partial v}{\partial t} + u\frac{\partial v}{\partial x} + v\frac{\partial v}{\partial y} + \frac{\omega}{d+\zeta}\frac{\partial v}{\partial \sigma} + fu = -\frac{1}{\rho}P_v + F_v + \frac{1}{(d+\zeta)^2}\frac{\partial}{\partial \sigma}(V_v\frac{\partial v}{\partial \sigma}) \qquad 3$$

$$\frac{\partial \omega}{\partial \sigma} = -\frac{\partial \zeta}{\partial t} - \frac{\partial[(d+\zeta)u]}{\partial x} - \frac{\partial[(d+\zeta)v]}{\partial y} + H(q_{in} - q_{out}) + P - E \qquad 4$$

In the previous equations, d is the depth of the water below a reference plane (m); f is the Coriolis parameter (1/s); Fu and Fv are the components x and y of the external forces (N/m²); u,v,w are the components x, y, z of the velocity (m/s); ρ is the specific mass of the water (kg/m³); Vv is the turbulent viscosity (m²/s); ζ(x,y) is the free surface elevation above the reference level (m); H(x,y)= d(x,y)+ ζ(x,y) is the total depth (m); t is the time; Pu is the component x of the pressure gradient (m/s); Pv is the component y of the pressure gradient (m/s), qin represents the local contribution of a source and $qout$ of a sink per unit volume (1/s), P is the nonlocal source term due to precipitation (m/s), *E* is the non-local sink term due to evaporation (m/s) and ω is the vertical velocity relative to the moving plane σ.

The vertical velocities ω in the σ -coordinate system are computed from the

continuity equation.

$$\frac{\partial \zeta}{\partial t} + \frac{\partial [(d+\zeta)U]}{\partial x} + \frac{\partial [(d+\zeta)V]}{\partial y} = Q \qquad 5$$

by integrating in the vertical from the bottom (-1) to a level (zero).

The depth is considered to be much smaller than the horizontal length scales of the phenomenon to be studied. Under the shallow water assumption, the vertical momentum equation is reduced to a hydrostatic pressure equation. Vertical accelerations due to buoyancy effects and due to sudden variations in the bottom topography are not taken into account (DELTARES, 2014), so:

$$\frac{\partial P}{\partial \sigma} = -g\rho H \qquad 6$$

This last equation provides a substantial simplification of the governing system of equation because the vertical distribution of pressure can be determined from the density field. It does not directly depend on the fluid motion (SOLOVIEV; LUKAS, 2006).

By integration of the equations 2 and 3 from the bottom to the free surface, the 2D (depth averaged) momentum equations arise. The continuity equation 5 already uses depth-averaged velocities.

To integrate the momentum equation it is necessary to assume: a non-stationary motion, so vertical velocity at the undisturbed sea surface z=0 is kinematically equal to the time derivative of the water level $\frac{\partial \zeta}{\partial t}$, so that $w|_{z=0} = \frac{\partial \zeta}{\partial t}$, and in a basin of variable depth H(x, y), a free-slip bottom boundary condition (missing velocity projection normal to the bottom) is: $w|_{z=-H} = -(u|_{z=-H} \frac{\partial H}{\partial x} + v|_{z=-H} \frac{\partial H}{\partial y})$.

In case of a two-dimensional depth-averaged model, the momentum equations reduce to:

$$\frac{\partial U}{\partial t} + U\frac{\partial U}{\partial x} + V\frac{\partial U}{\partial y} + fV = -\frac{1}{\rho}P_u + F_u + \frac{\tau_{sx} - \tau_{bx}}{\rho(d+\zeta)} \quad 7$$

$$\frac{\partial V}{\partial t} + U\frac{\partial V}{\partial x} + V\frac{\partial V}{\partial y} + fU = -\frac{1}{\rho}P_V + F_V + \frac{\tau_{sy} - \tau_{by}}{\rho(d+\zeta)} \quad 8$$

being τ_s and τ_b bed and surface stress.

Time derivative of water level depends on the divergence of volume transport. When the volume transport is directed towards the coast then water level will rise (ELKEN).

This set of partial differential equations, in combination with an appropriate set of both initial and boundary conditions, is solved on a finite difference grid.

Within Delft-3D, there is the hydrodynamic module Delft3D-FLOW, which is a tool simulate two-dimensional (2D, depth-averaged) or three-dimensional (3D) unsteady flow and transport phenomena resulting from tidal and meteorological forcing, including the effect of density differences due to a non-uniform temperature and salinity distribution (density-driven flow) (GERRISTEN et al., 2007).

It aims to model flow phenomena of which the horizontal length and time scales are significantly larger than the vertical scales, which is the so-called shallow water assumption.

The areas of application are extensive, such as: tide and wind-driven flows (i.e. storm surges), stratified and density driven flows, simulations in deep lakes and reservoirs, fresh-water river discharges in bays, salt intrusion, thermal stratification in lakes, seas and reservoirs, cooling water intakes and waste water outlets, online sediment transport and morphology, etc (DELTARES, 2014).

3.2.2 Initial and boundary conditions

The solution of the equations above, for shallow waters, consists in moving from a physical-mathematical model to a numerical model in which the equations are solved with certain initial and boundary conditions (JUÁREZ, 2014).

- Boundary Condition

An open boundary can be forced by astronomical tide, using the tide harmonics. The following types of boundary conditions are available: water level, velocity, Neumann (water level gradient), discharge or flux (total or per grid cell) and Riemann or weakly reflective boundaries. The choice of the type of boundary condition used depends on the phenomena to be studied.

Neumann's boundary condition type is used to impose the value of the normal gradient to the boundary of any function. An example may be the imposition of the water level gradient that is normal to the coastline. Neumann boundaries can only be applied on cross-shore boundaries in combination with a water level boundary at the seaward boundary, which is needed to make the solution of the mathematical boundary value problem well-posed.

Wind, in many places, is responsible for producing surface currents as well as vertical mixing under special conditions (FISCHER et al., 1979). In shallow water bodies, winds can be a really important forcing factor in hydrodynamic studies.

The wind drag coefficient may be linearly dependent on the wind speed, reflecting increasing roughness of the water surface with increasing wind speed. The three wind drag coefficients determine three breakpoints in the piece-wise linear function of wind drag coefficient and wind speed. In this work, the formula of Large and Pond (1981), was employed to determine the breakpoints.

Large and Pond (1981) developed a simple algorithm consisting of a bulk formula for calculating the drag coefficient using only the wind velocity:

$$C_{D,LP} = 1.2 \times 10^{-3}, for\ 4 \leq \bar{V} < 11m/s \quad (9)$$

$$C_{D,LP} = (0.49 + 0.065\,\bar{V}) \times 10^{-3}, \ \ for 11 \leq \bar{V} < 25m/s \quad (10)$$

where $\bar{V}$ is the absolute value of the wind velocity, and $C_{D,LP}$ is the drag coefficient. This formula relates the drag coefficient (and consequently also the wind stress) only to the wind speed (LARGIER et al., 2006). This algorithm has been used in many studies such as (DORMAN et al., 2018).

At the free surface the boundary conditions for the momentum equations are:

$$\frac{v_H}{H}\frac{\partial u}{\partial \sigma}|\sigma_{=0} = \frac{1}{\rho_o}|\overrightarrow{\tau_s}|\cos(\theta) \quad (11)$$

$$\frac{v_H}{H}\frac{\partial v}{\partial \sigma}|\sigma_{=0} = \frac{1}{\rho_o}|\overrightarrow{\tau_s}|\sin(\theta) \quad (12)$$

where θ is the angle between the wind stress vector and the local coordinate direction. Without wind the free surface stress is zero. The magnitude of the wind shear-stress is defined as:

$$|\overrightarrow{\tau_s}| = \rho_o \vec{u}_{*s}|\vec{u}_{*s}| \quad (13)$$

The magnitude is often determined by the following widely used quadratic expression:

$$|\overrightarrow{\tau_s}| = \rho_o C_d U_{10}^2 \quad (14)$$

in which U10 is the wind at 10-meter height. Wind effort can be applied either uniform or space varying. The latter is generally applied in combination with space and time varying atmospheric pressure. At the sea bed, the boundary conditions for the momentum equations are:

$$\frac{v_H}{H}\frac{\partial u}{\partial \sigma}|\sigma_{=-1} = \frac{\tau_{bx}}{\rho} \quad (15)$$

$$\frac{v_H}{H}\frac{\partial v}{\partial \sigma}|\sigma_{=-1} = \frac{\tau_{by}}{\rho} \qquad 16$$

with τ_{bx} and τ_{by} the bed stresses in x- and y-direction, respectively. The bed stress may be the combined effect of flow and waves.

- Bottom Friction

Lagoons and coastal semi-enclosed basins morphologically evolve depending on local waves, currents, and tidal conditions. In very shallow water depths, typical of tidal flats and mudflats, the bed shear stress due to the wind waves is a key factor governing sediment resuspension.

The interaction between the local flow and a moving bottom induces a shear stress that, depending on the physical characteristics of the bottom material, may result in resuspension and subsequent sediment transport and/or drag transport.

3.3 Previous studies

Baptistelli (2008), made a critical analysis of the use of mathematical modelling in the dispersion of effluents in the Estuarine System of Santos - São Vicente, Brazil, using three different models for the simulation of local hydrodynamics. When comparing the results of hydrodynamic simulations performed through MIKE 21, POM and Delft3D, better results were obtained from the Delft3D model, with a correlation coefficient of 0.8, while for the other models a value of 0.63 was obtained and 0.7, respectively.

The results of Baptistelli (2008), indicate the Delft3D model as a good option for hydrodynamic modelling of estuarine environments, which still has the advantage of having several modules available for joint use, such as sediment transport and water quality.

Many estuaries world wide are becoming more urbanized with heavier traffic in the water ways, requiring continuous channel deepening and larger ports, and increasing suspended sediment concentration (SSC).

An example of a heavily impacted estuary where SSC levels are rising is the Ems Estuary, located between the Netherlands and Germany. The channel of this estuary has been deepened by dredging over decades. Van Maren et al. (2014), used a numerical model of suspended sediment transport forced by tides, waves and salinity. To determine the impacts of the dredging activities, a 3D numerical model was implemented using the Delft3D free software.

The model satisfactorily reproduced observed water levels, velocity, sediment concentration and deposition in the estuary. Therefore, was subsequently applied to test the impact of channel deepening, historical dredging strategy and port construction on SSCs in the Estuary.

The time series obtained for water elevation where compared in 4 stations, while flow velocity was for a period of 5 months at two stations. After calibration, the sediment transport model was incorporated.

A time-series comparison of the computed and observed suspended sediment concentration were also compared with a station. They reported large deviations of the model for sediment concentration, mainly for the months of February and November. The underestimation of the concentrations was attributed to de complexity of the Ems River sediment transport processes.

The most realistic way to evaluate the effect of the presence of ports (excluding their approach channels) is by comparing the model including ports and subsequent dredging and disposal activities (the reference model), with a scenario without ports (and therefore also without deposition in ports nor related dredging and disposal activities).

Finally, they concluded that the long-term impact of dredging on suspended sediment concentrations has received limited attention in scientific literature. The long-term morphological effects of dredging are fairly well known due to the relatively large amount of (historic) topographic data in heavily modified estuaries.

Most commonly, studies related to dredging-induced turbidity focus on the sediment dynamics in the direct vicinity of the dredger (PENNEKAMP et al.,1996)

on the fate or deposition of dredged sediment (e.g. DELEU et al., 2004) or on the impact on sensitive ecosystems (ERFTEMEIJER; LEWIS,2006).

Tobón (2002) proposes a calibration of the Delft3D hydrodynamic model based on the evaluation of the sensitivity of water level and velocity results in relation to grid spatial resolution, time step, 3D or 2DH domain representation, boundary conditions, bathymetry, bottom roughness, turbulent viscosity and local wind.

He also studied the flows along the tidal channels, and the influence of the modified bathymetries along time as well as the influence of the bottom roughness.

The conclusions of his research where that the bottom roughness, even in the deepest areas, has a great influence in the flow velocities. The bathymetry had a great effect on the water level and into the volumetric rate in the monitored section areas. The bottom roughness as well as the bathymetry had a determinant effect on the model results, being an important factor to take care of during calibration process.

In Cádiz Bay, Spain, Delft3D-FlOW module was used to simulate the future response to human interventions (a project that will deepen the main channel is developing), and to understand their impacts on the bay. In particular, the investigation was focused on the effects on the hydrodynamics and the sediment transport patterns. Zarzuelo et al., (2015), obtained great results with this applied model, concluding that the interventions have a relatively large impact on the bay hydrodynamics, which is most obvious for the tidal flow and the residual current. The results indicate that the ability of the bay to exchange water and transport sediment between the inner and outer bay will deteriorate, thus impacting the ecological environment of the bay. For example, the changes could promote sedimentation in the inner bay due to the lower current velocities.

Lacerda (2016), used the Delft3D numerical model to simulate hydrodynamics and sediment transport, and to analyze the possible impacts caused by deepening the access channel to the port of Vitoria, Espirito Santo, Brazil. The numerical model satisfactorily reproduced the observed elevation, velocity,

temperature, salinity and concentrations of suspended sediment data in the Bay of Vitória. The results suggest that the deepening of the channel drives in a greater localized impact, inducing a reduction in flow velocities, concentrations of suspended sediment and erosion and deposition values over the in-depth region.

Although Lacerda (2016) obtained a decrease in flow velocity in response to the dredging of the port channel of Vitoria, Espirito Santo, Zarzuelo et al., (2015), found that after dredging activities in the Bay of Cádiz, Spain, the residual currents would increase, resulting in an increase in the erosion and deposition of sediments. Erosion is expected to occur on the banks and close to the intervention, whereas deposition mainly affects near-channel areas.

3.4. Studies in San Quintín Bay

The study of the hydrodynamics of the BSQ gained momentum during the 80's, then; the tide was identified as one of the main forces of circulation, followed by the effort of the wind (CHANES, 2016).

Lucero (1979), in 1979 presented a 1D hydrodynamic study of the San Quintín Bay Lagoon. The model was useful in understanding the horizontal and vertical movement at the mouth of the lagoon, which was determined as non-homogeneous, with a horizontal gradient W-E of the input speeds.

Lucero (1979) determined through statistical analysis and numerical modelling, that the effort of the wind does not have a significant response on the circulation of water in the lagoon system whose influence is restricted to the surface layer in the main channels; however, Gómez (1980) found a more significant response only in the open areas of FB and head of BSQ. Likewise, Oxamendi (1989) confirmed the importance of wind forcing on the variability of residual circulation in periods of 4 to 21 days.

Lucero and Muro (1977), applied a one-dimensional numerical model to reproduce the hydrodynamics of the lagoon, based on observations made during the summer of 1977. The model proved to be little predictive. For this location, it

was recommended the use of 2D models and the numerical method of finite elements instead of finite differences.

Vidal (2006), studied the pattern of residual circulation in the BSQ using data from ADCP's (Acoustic Doppler Current Profilers). He recognizes a circulation divided into two layers, the surface layer being mostly influenced by the winds and the lower layer by the tides. When the wind is weak the two layers circulation is inhibited giving rise to a homogeneous circulation in the whole column of water and modulated by the tide.

He also reported that the Baja California coastal upwelling system is induced by winds from the N and NW, parallel to the coast; these winds are combined with terrestrial rotation to induce a transport of surface water out of the coast, which is replaced by deeper waters that are colder, denser and nutrient-rich.

Ibar et al., (2009), evaluated the effect of upwelling in the BSQ as well as the effect of the tide on some nutrients. They evaluated by fieldwork: salinity, temperature, nitrates, pH and Ct. They report a temperature gradient between the east arm of the BSQ and the mouth of the lagoon of approximately 7 ° C.

González et al., (2012), presented a 2D numerical model of the hydrodynamic regimes at BSQL, that considers the wind effect as well as analyzing food input to the lagoon, residence times and waste production within the lagoon by using a lagrangean tracker method. The hydrodynamics regimes and waterborne particle transport was obtained using the Coastal Modelling System Flow (CMS) Flow in conjunction with the Particle Tracking Model (PTM).

The model domain was defined for the whole lagoon as well as an open water area which acts as a buffer zone between the lagoon and the forcing boundary, and the grid is composed of 105,966 rectangular cells with size of 50 by 50 meters each and it has an azimuthal rotation of 333°. The domain bathymetry was created using data reported by Vidal (2006) and actualized with data collected 2009, 2010 and 2011 field work experiments; data set is referenced to mean low level water.

They found that the majority of the lagoon is shallow (between 0.5 m and 1.5 m), and that the main forcing processes within the lagoon are tide, most important, and wind (of secondary importance). They also reported that the best fit with the observed dispersion rate was obtained using a 0.6 m2/s coefficient.

García et al., (2014), made a study with the objective of demonstrate that OpenDA could be used effectively to rapidly calibrate a hydrodynamic model for smaller sub-meso scales like the size of San Quintin Bay Lagoon.

They presented two methods of reducing the uncertainty within the models: calibration, with a goal of tuning a set of parameters that are fixed in time, and data assimilation, with the goal of improving the starting position of the forcing for a forecast, so that the estimates are different in each cycle.

They used Delft3D software for the hydrodynamics model, focus in a local scale problem where the open-boundary plays a very important role as well as the dynamics at the entrance.

This work presented the details regarding how OpenDA is used to calibrate the parameters at any depth or friction, as well as the components of the tides in SQB. One of the objectives of this work was to show when the numerical model is unable to capture the physics of its region of study. In such cases, the correlation is low, and OpenDA plays an important role in the model calibration.

García et al. (2014) concluded that the Delft3D model is capable of reproduce the essential processes in the BSQ, and can be forced by the tidal model and wind. Conversely, diurnal and semidiurnal components at the boundaries show that a change in their parameter have an important role in the dynamic of the bay. Calibration using OpenDA in a small-scale problem, did improve the first model implementation showing that friction and changes in depth were not significant.

While tide and wind forcing are the main forces that move the hydrodynamics inside the bay, the depths average velocities for the 3D runs shows that Delft3D and OpenDA calibration in 2D was enough to explain the variability in currents along the bay with a very high correlation during the period of time considered, and there was no need to calibrate any other parameters for the 3D model. At the

bay entry we found the main direction is NNE during high tide and SSW during low tide with a higher magnitude in this direction.

For this study, the astronomical tide, H(t), due to the eight primary harmonic constituents (A and G) of the semidiurnal (M2, S 2, N2, K2) and the diurnal (K1, O1, P1, Q1) was obtained from a global model of ocean tides. On the other hand, a classical tidal harmonic analysis including error estimates using [18] was done to the pressure time series at the bay entry in order to find the more predominant components of the tide in the region (results are shown in Figure 3). An estimation of the tidal amplitude and phase with 95 % interval confidence shows that the predominant components are K1, 01, M2 and S 2 .

Chanes (2016), applied a 3D hydrodynamic model (ELCOM), which coupled a biogeochemical model of water quality (CAEDYM). Both models were fed with data obtained directly in the field. His work is the pioneer in terms of nutrient dispersion by hydrodynamics and does not consider the variation of nutrients by zooplankton, fish and oysters.

She used bathymetric data from a previous work done by Vidal (2006), who measured the depths through various routes to cover most of the interior of BSQ and completed with ETOPO2 satellite data. Chanes (2016), created a 2D cartesian mesh of 100 x 100 m in the horizontal, and with a variation of 0.5 - 10 m in the vertical.

It used astronomical tide prediction for May and June 2004. For atmospheric conditions, data were obtained from a meteorological station that measured solar radiation, air temperature, atmospheric pressure, wind speed and direction. The time series were applied homogeneously over the whole domain and, therefore, it is important to consider certain possible changes in hydrodynamics.

The simulation period was 63 days with a time step of 30 seconds. The residence time was also calculated. The validation of the hydrodynamics was carried out by comparing the currents (magnitude and direction) obtained against measurements obtained in the field through an ADCP (acoustic profiler of

currents by Doppler effect) reported by Larios (2006). There was also compared temperature and salinity values obtained in the simulation with real values of measurements reported by Camacho-Ibar et al. (2007).

Chanes (2016), mentions that the model was incapable of assimilating the friction of the bottom and could have repercussions on the currents that change with the hydrodynamics. It is believed that the variations between the data simulated by ELCOM and those measured in the field is mainly due to the fact that meteorological parameters such as wind and solar radiation were applied homogeneously throughout the domain.

The 3D model that was implemented, describes the general hydrodynamics including the residual circulation of the entire simulation, the diurnal and biweekly variability of the system and the residence time. According to the simulation, currents of greater magnitude occur on the surface. Some authors suggest that it is due to the effect of wind on the surface of water.

Vidal (2006) reports that the circulation in BSQ is essentially controlled by the tide, where it explains 95% of the magnitude of the velocity of the currents measured in the bottom, while in the surface they explain 70%. As reported by Chanes (2016), the speeds inside the bay do not exceed 0.4 m / s. Larios (2006) and Vidal (2006) recorded speeds of 0.1 m / s.

Chanes (2016), reports that the use of ELCOM generates overestimation in the magnitude of the currents, particularly in the region of the mouth and part of the central channel where speeds reach 0.3 m / s. An advantage reported by Chanes (2016) with ELCOM is the ability to generate changes in the coverage area due to the variation in sea level, the coastline increases at high tide and is reduced at low tide.

Regarding the currents within the BSQ, Juarez (2014), through a numerical simulation recorded residual currents up to 0.18 m / s on the surface. While Juarez (2014) reported that, during high tide, cooler water from the ocean ventures through the bottom and stratifies the water column, Chanes (2016), obtained different results which demonstrate a well-mixed water column for both high tides as low tides.

Chanes (2016) reported that both temperature and salinity inside BSQ show a gradual increase in their values towards the north (in the arm this salinity reaches values of 37), behavior also reported by Ibar et al. (2007).

Chanes (2016) detected that the highest temperatures are found in the western arm (False Bay). The highest temperature values where found towards the north in both arms. This is attributed to a high rate of evaporation, shallowness and longer residence times (BORREGO et al., 1982). Chanes (2016), reports vertically homogeneous water column for salinity and temperature with minimum stratification within the BSQ.

Vidal (2006), state that in bays or coastal lagoons where vertical density gradients are negligible, as is the case of the BSQ, it has been shown that the dynamics are due to tidal forcing, wind and bathymetry mainly.

Hernández (2005), by means of a two-dimensional model that had forcing the wind and the tide, determined that the residence times of the BSQ were around 5 days for BF and 15 days for BSQ, while Chanes (2016), through ELCOM, reported longer residence times of up to 5 days for BSQ in both arms.

For the use of ELCOM within the BSQ, discrepancies were reported between the simulated results and the data measured in the field due to the tiered grid (without slopes or smoothed boundaries) (CHANES, 2016). ELCOM presented errors when overestimating residence times. Regarding circulation, ELCOM coincided with the theory of anti-estuarine circulation characteristic of hypersaline lagoons where outflows occur in deep parts and inlet in shallow areas.

The decrease of the average density in the mouth direction towards the head of the eastern arm (San Quintin Bay arm), allows to infer a slight contribution to the residual or subtidal circulation, leaving through the surface (t = 23.27) and entering water from the adjacent sea through the bottom (t = 26.04) (DÍAZ, 1980). Within BSQ, the maximum calculated residual current values were 18 cm / s at the surface and 9 cm / s at the bottom (LARIOS, 2006).

4. METHODOLOGY

4.1 Study Area

The San Quintín Bay Lagoon (SQBL) is a coastal lagoon located in the Mexican State of Baja California between 30° 24' and 30° 30' north latitude and 115° 57' and 116° 01' west longitude, and covers an area of approximately 42 km2. This lagoon is one of the most important coastal lagoons at the Pacific of Baja California and is characterized by its high capacity of aquaculture and agricultural production (GONZALEZ et al., 2012). The lagoon is divided in two basins: the eastern arm named San Quintín Bay (same name of the lagoon but different abbreviation: SQB), and the western arm named False Bay (FB).

The mouth of the lagoon is 1 km wide and has maximum depth of 14 m (GONZALEZ et al., 2012): the connection to the open sea is free, it means that

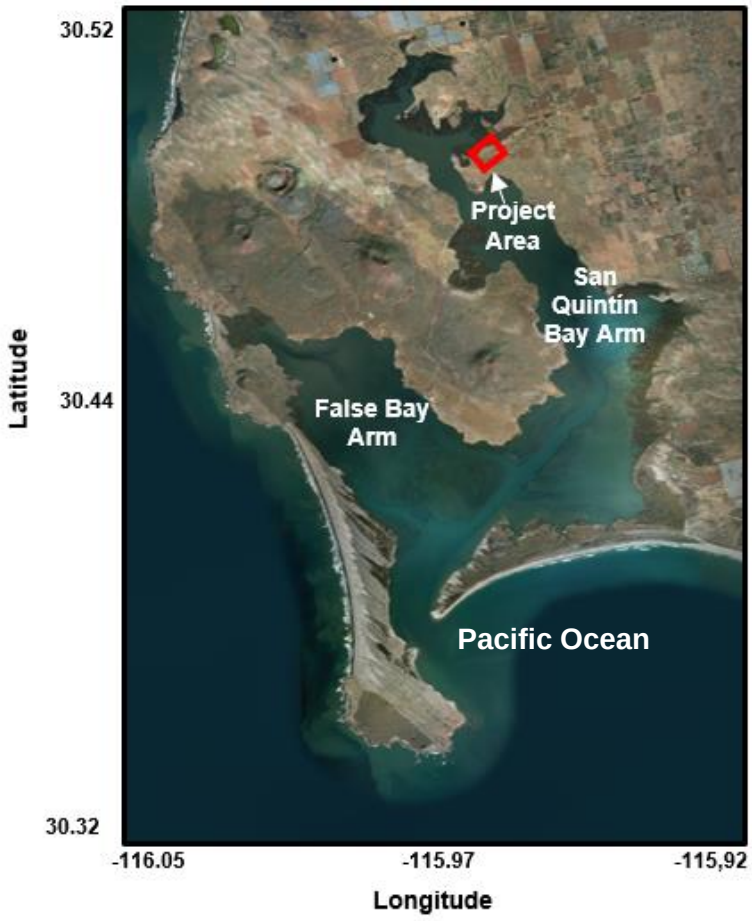

Figure 2. Geography of San Quintin Bay Lagoon (SQBL)

the communication between the ocean and the lagoon should allow the exchange of water, salt, and the transmission of tidal energy permanently for all tidal conditions and during all seasons of the year.

The bars that divide the lagoon from the ocean (west and south) are mainly composed of sand with few gravel areas north of the west bar (JUAREZ, 2014). Approximately 70% of the lagoon bottom is of mud-flat character with a mean depth of 2 m. Extensive development of vascular plants, dominated by Zostera marina, occupies the greater part of the muddy bottom.

These areas of the lagoon consist mostly of very shallow sand and silt lows, intertidal flats with seagrass beds, marshes and narrow tidal channels; that do not exceed 15 m deep, with reference to the Mean Lower Low Water (BORREGO; BORREGO, 1982).

The SQB (eastern arm) has a narrow channel, whose maximum depth in the transverse transects, can reach more than 10 m in depth, until the vicinity of El Molino Viejo (Figure 2). From this point and to the head of SQB, a channel of 2 km extends, which is subject to flooding by the tide (SERVICIOS TURISTICOS Y PESCA COMERCIAL LOS VOLCANES SPR DE RL, 2014).

Tides in the north Pacific coast are the primary hydrodynamic forcing agent for coastal lagoons. The most intense tides occur during spring tides while the less exchange occurs during neap tides (GONZALEZ et al., 2010).

The tide that is observed in any location is the superposition of several constituents that come from the different forcing mechanisms (celestial bodies). The main constituents for the San Quintin Bay Lagoon were identify after performing an analysis of tidal harmonics (Figure 3).

The main harmonics that govern the tide are seven: M2, S2, K1, O1, N2, P1 and K2.

For a period between May and June, according to measurements made by Larios, 2006, affirmed that these constituents contribute with 95.5% of the total energy, being M2 the dominant with 37%.

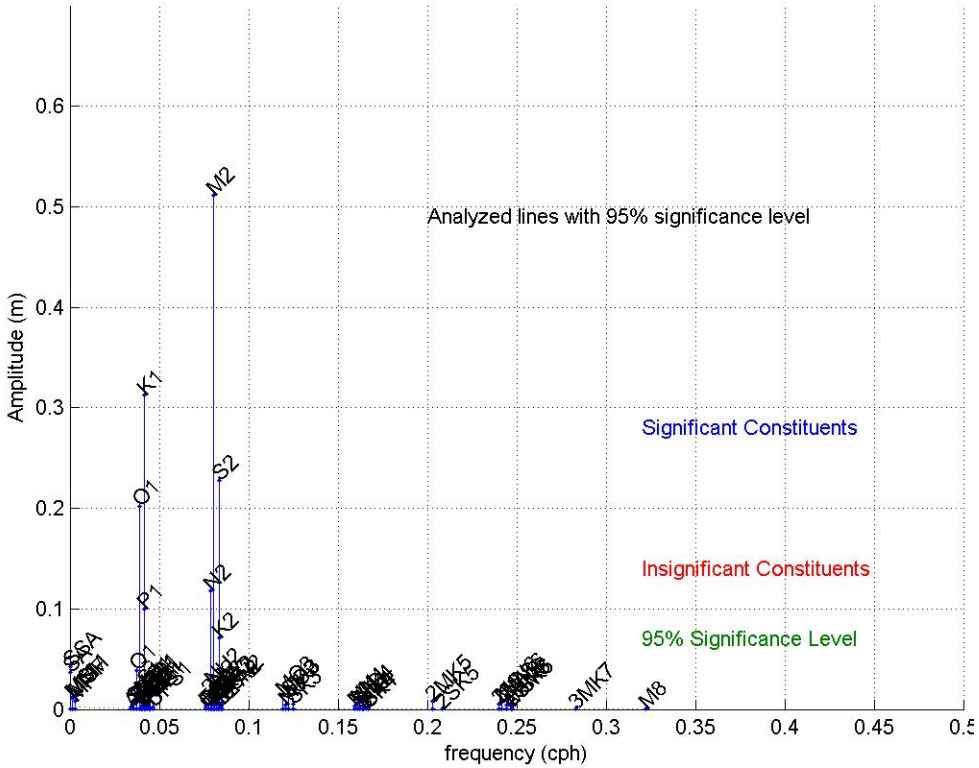

Figure 3. Harmonic tidal analysis for San Quintin Bay Lagoon

The constituents were used to characterize the tidal regimes present in the study area using the Courtier coefficient "F", or better known as the form factor (BRAVO R. et al., 2000):

$$F = \frac{Amplitude\ K_1 + Amplitude\ O_1}{Amplitude\ M_2 + Amplitude\ S_2} \qquad 17$$

The form factor for the San Quintin Bay study region showed a value of F ~ 0.72, which means that the tidal regime is mixed semidiurnal with amplitudes as high as 1.6 m above MLLW (Mean Lower Low Water) during spring tides, as reported by Gonzalez et al., 2012. There is a 40 minutes tidal lag between the lagoon mouth and the head in BSQ, located in the inner part of the right arm of SQBL (TORRES, 1980).

Water temperature at SQBL shows a clear seasonal signal and a clear variation

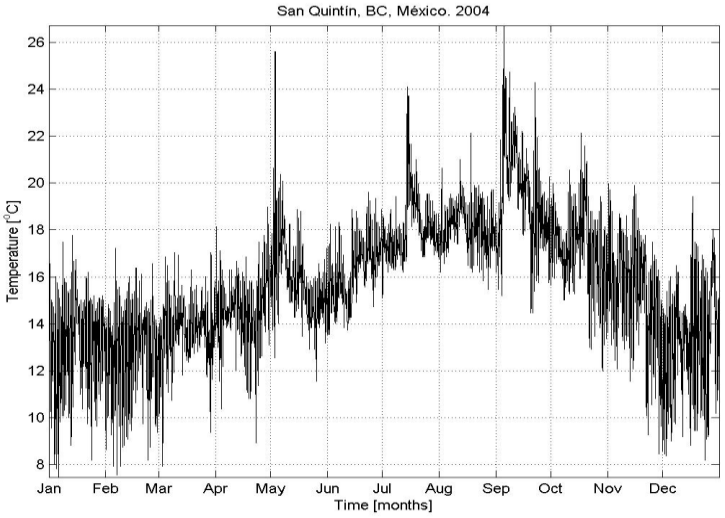

Figure 4. Temperature air behavior during 2004 for the San Quintín Bay Lagoon.

between FB and SQB and throughout a tidal cycle, and within its shallow areas the water temperature closely tracks air temperatures even with the constant effects of wind mixing processes. During the year, temperatures varies between 8º (Celsius degrees) for winter and goes up to a maximum of 27º during summer. According to Borrego and Borrego, 1982, the BSQL is considered as a vertically mixed system, that is, there are no significant vertical gradients of temperature or salinity in the bay.

The shallowest of the east arm of the lagoon (SQB), was pointed out as one of the biggest limitations to navigate in the lagoon. As mentioned before, exists an intention of deepen the area known as Molino Viejo to create a small port. The purpose of the deepening of the Molino Viejo area is to enable the transport and parking of small boats, thus increasing tourism. The volume expected to be dredged is approximately 2,752.75m³.

BSQL is located in an arid and volcanic zone. The climate is Mediterranean; therefore, evaporation rates are high. The lagoon has sporadic river supply and minimal rainfall (BORREGO, et al., 1975), however, BSQL is a region considered highly productive. In the particular case of San Quintin Bay Lagoon, the wind is

generally strong, with a yearly average of approximately 3.5 m/s, and the direction does not change very much during the year (315º), thus, being also an important forcing agent for the lagoon hydrodynamics. Northwest surface dominant winds with a frequency of 72.5% (BORREGO; BORREGO, 1982).

Figure 5 shows a wind rose for the measurement period. The segments indicate the quadrant from which the winds blow, according to the meteorological convention, the colors indicate the wind intensity [m/s] and the segmented circles correspond to the frequency of occurrence of the data, in percentage (%).

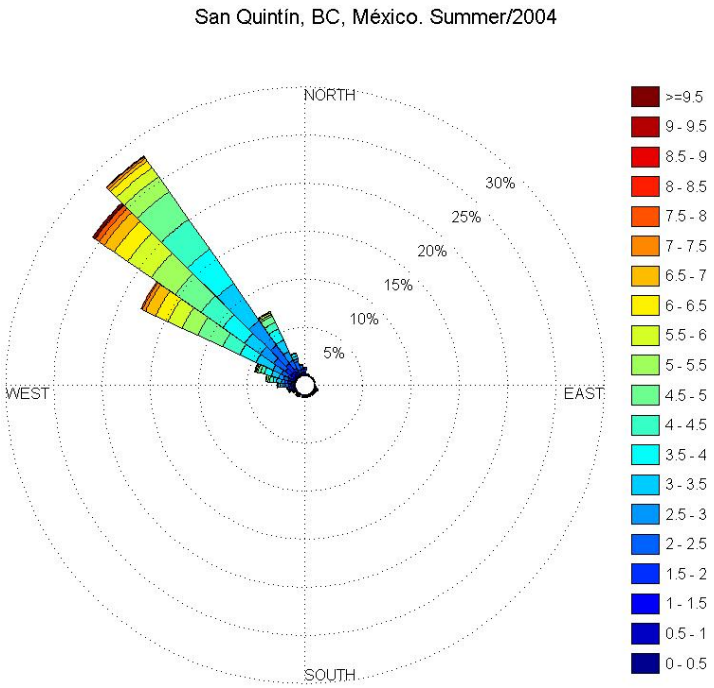

Figure 5. Wind Rose for San Quintin Bay Lagoon during Summer for 2004

It can be appreciated that the wind does not change very much, as said before, presenting a dominant direction. A similar study in SQBL, Baja California, revealed a 15% contribution of the meteorological tide to the total tide due to a more pronounced effect of the local wind in that place.

Diaz (1980), using temperature and salinity data, suggested a horizontal circulation pattern due to density gradients. He found that the density horizontal structure depends on the temperature, which implies that the heating-cooling process is dominant over the evaporation process, and in most cases, the waters

of the bay are less dense towards the head than in the mouth, creating a horizontal gradient increasing concentration rates of temperature and salinity towards the north of the lagoon.

On the other hand, the vertical density gradients in BSQL are minimal, because there are no significant freshwater contributions. Even when the evaporation and salinity are high, a vertical structure cannot be formed due to the effects of the tide (mixture) (DÍAZ, 1980; OXAMENDI, 1989).

The Pacific coast of the Baja California Peninsula is located in one of the four coastal upwelling regions (California, Peru, Benguela and the Canary Islands) with the highest primary productivity per unit area worldwide. Baja California's coastal upwelling system is induced by winds from the N and NW, parallel to the coast; that combine with the earth's rotation to induce a surface water transport out of the coast, which is replaced by sub-surface waters that are colder, denser and rich in nutrients.

The current dynamics of the coastal oceanographic system surrounding Baja California is dominated by the influence of the California Current (CC), which affects the coast of Baja California between 29 ° N to 30 ° N and then continues its journey to the south along meanders and turns (ALCAZAR, 2008).

4.2. Hydrodynamic model: Delft3D-FLOW

4.2.1 Data collection

Wind

To apply the wind effort, the Oceanographic Research Institute (IIO) from the Autonomous University of Baja California (UABC), provided a report of the measurements of wind speed and direction recorded at a weather station located in San Quintín, Baja California [30.5317 oN, 115.8375 oW] owned by the National Meteorological Service. The observation period was from January to December 2004.

The wind drag coefficient (Cd) is set according to the wind speed at ten meters, and may be linearly dependent on the wind speed, reflecting increasing roughness of the water surface with increasing wind speed. This increase is

greater in shallow water than in deep water (SMITH et al., 1992) and formulations have been proposed for decades by several authors (SMITH; BANKE 1975; GARRATT, 1977; LARGE; POND, 1981; KUMAR et al., 2009). In this case, the Smith and Banke, 1975, equation was used:

$$103\ Cd = 0{,}63 + 0{,}066\ U10 \qquad 18$$

Where Cd is the drag coefficient and $U10$ is the velocity at 10 meters.

Sea level and currents

Data measured in field for sea level and velocities were provided by the Oceanographic Research Institute (IIO) of the Autonomous University of Baja California (UABC), during a campaign carried out in 2004. Three ADCP's were placed inside the lagoon (Figure 6), measuring sea level and currents. For sea level and currents, the ADCP's collected data for a period of time from 23-05-2004 until 13-06-2004, with a time interval Δt = 10 mins.

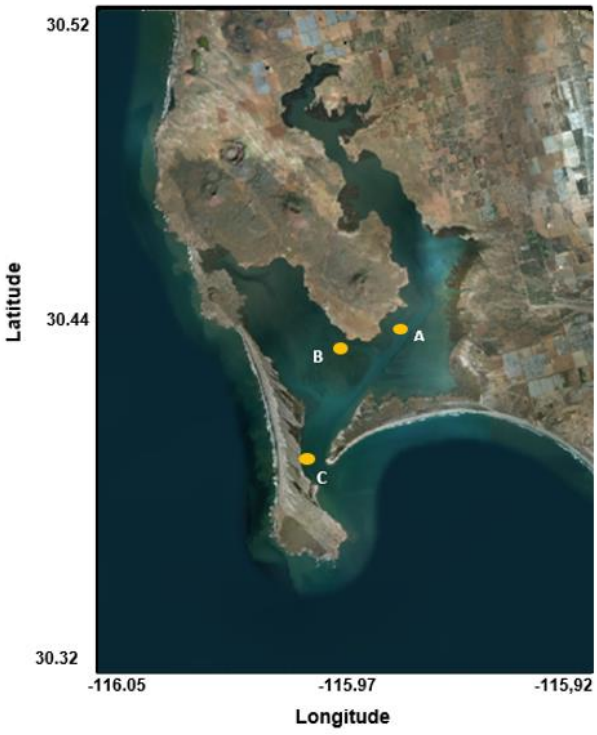

Figure 6. ADCP's localization: yellow dots

4.2.2. Implementation

4.2.2.1. Mesh

Because the lagoon has a complex bathymetry, an orthogonal mesh of variable dimensions was created. The area of the lagoon was refined locally (40 m x 120 m) to obtain a higher resolution, mainly in the principal deeper channels of the lagoon, while the area corresponding to the open ocean has a lower resolution (from 101.5m x 140 m to 1013m x 760m in the furthest areas). The total elements of the mesh were 11079 (Figure 7).

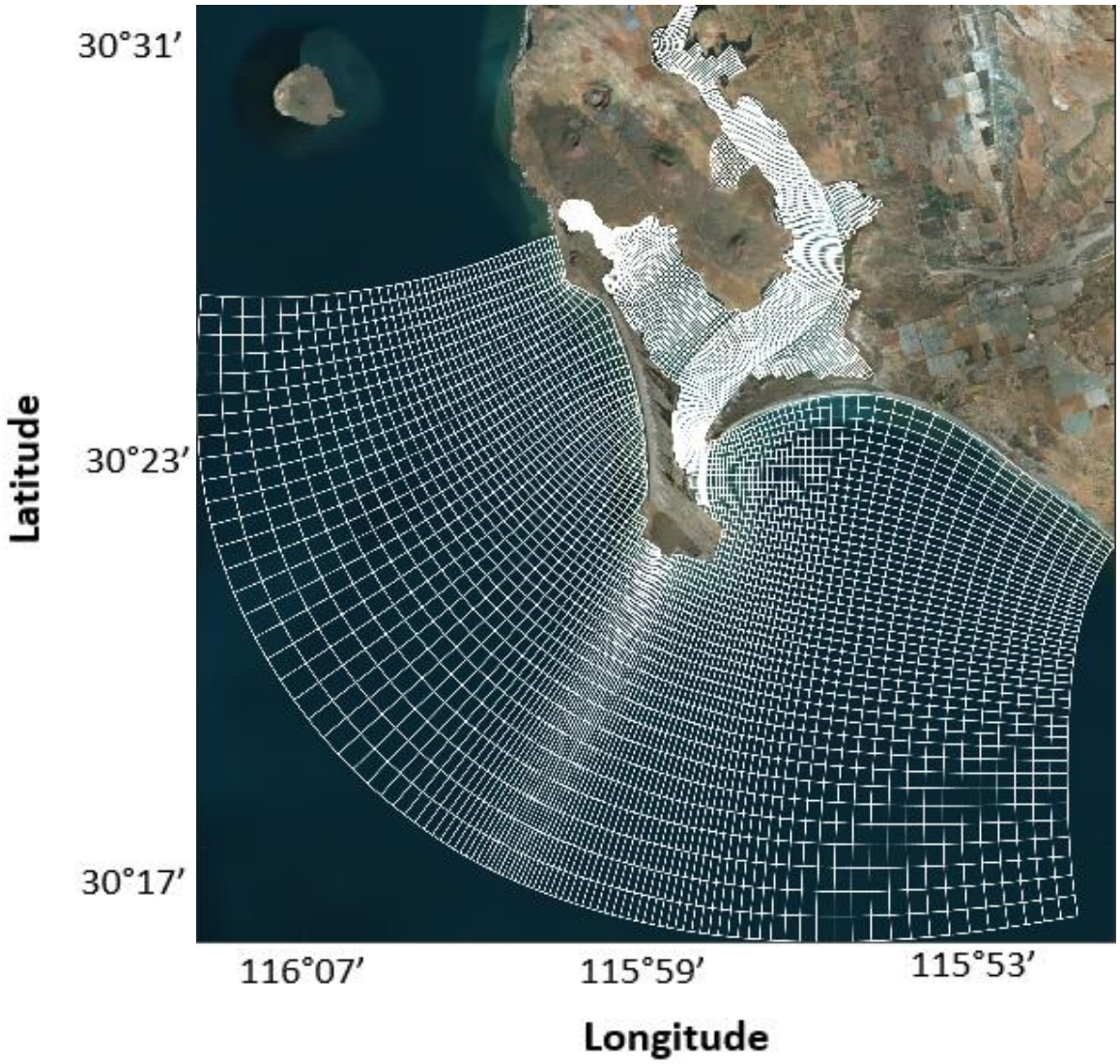

Figure 7. Orthogonal Mesh

4.2.2.2. Bathymetry

For the area of the lagoon, the bathymetry was obtained from measurements made in 2004 by the Oceanographic Research Institute (IIO), from the Autonomous University of Baja California, México (UABC). The bathymetry far from the coast was taken from GEBCO (The General Bathymetric Chart of the Oceans) (Figure 8) and both bathymetries were interpolated in the orthogonal mesh.

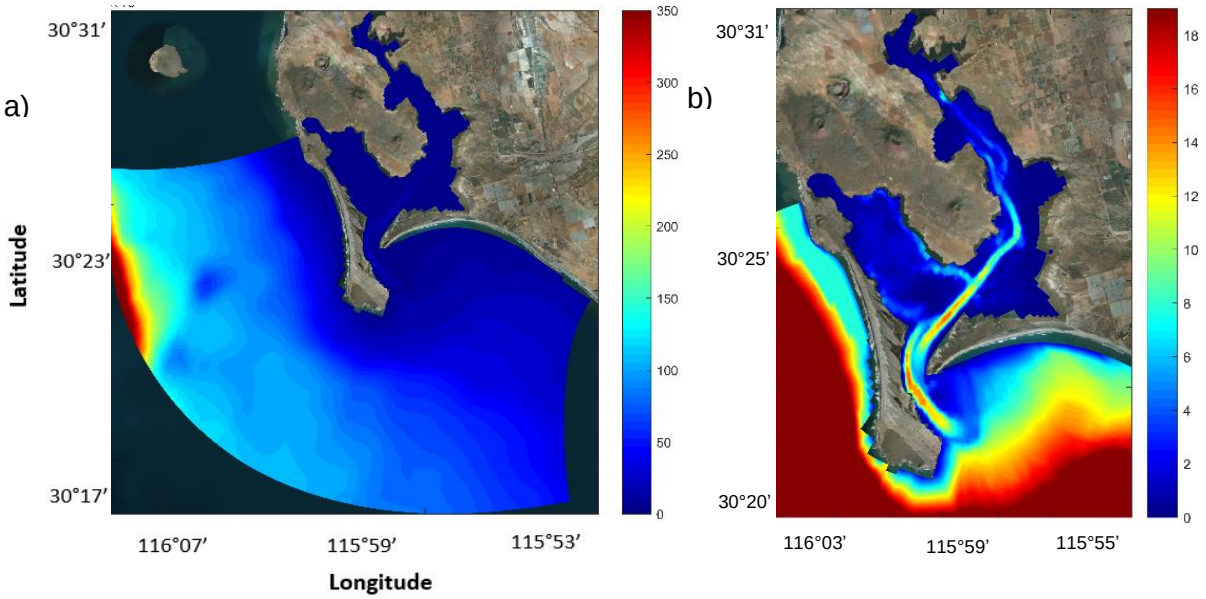

Figure 8 a) General interpolated bathymetry, including area of the open ocean, b) Local Bathymetry of the coastal lagoon BSQ

4.2.2.3. Initial and Boundary Conditions

Initial Conditions

Initial conditions are required for all dependent variables, such as water level and flow velocity components. For complicated topographies with large drying and flooding areas, which is the San Quintin Bay Lagoon case, is recommended to start running the model with high values for water level. The model was first started with a high-water level of 1.9 m. This was because at a maximum amplitude the velocity is consider zero. The uniform initial conditions for the flow velocity components in both horizontal directions were zero.

Open Boundaries

Major external forcings to surface waters include (1) atmospheric forcings, (2) point and nonpoint sources, and (3) forcings from open boundaries (GANG JI, 2008). In this work, the first and third external forcings were considered.

The flow may be forced using water levels, currents and the Neumann or Riemann condition. The hydrodynamic forcing can be prescribed using harmonic or astronomical components or as time-series.

Three open boundaries were specified (Figure 9): North, West and South. For this case, the Neumann type of boundary was used in the North and South boundaries, since it simulates a weakly reflective boundary. The main characteristic of a weakly reflective boundary condition is that the boundary up to a certain level is transparent for outgoing waves, such as short-wave disturbances.

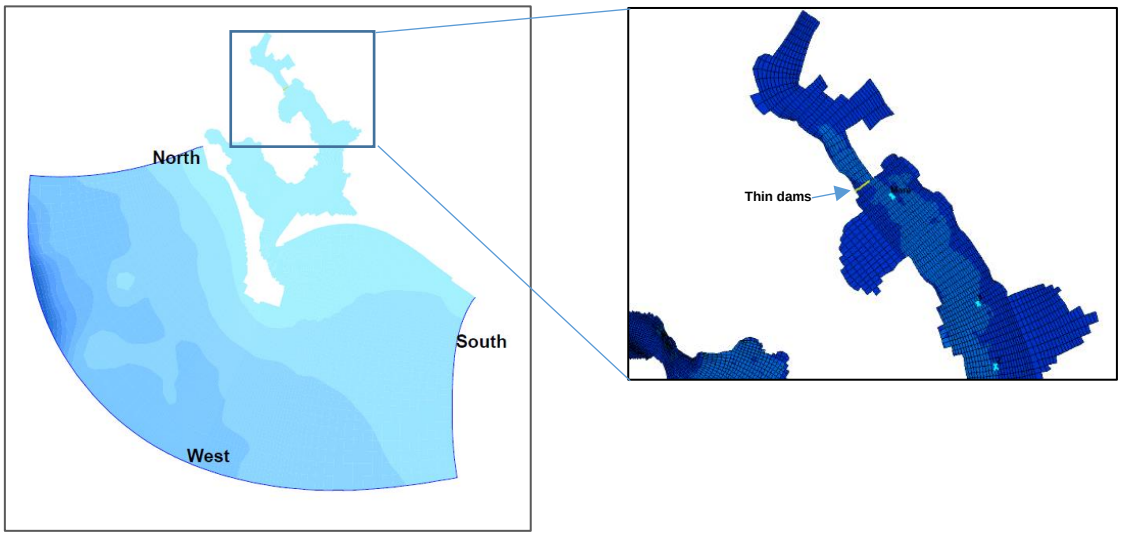

Figure 9. Open boundaries for the domain

For the West boundary, the astronomical tide due to the seven primary harmonic constituents of the semidiurnal (M2, S2, N2, K2) and the diurnal (K1, O1, P1) were used to force the model (these astronomical components were obtained

from a tidal analysis). Ramirez, et al. 2014, found the following values for the main harmonics, after performing calibrations applying DUD (a derivative-free algorithm for nonlinear least squares) and OpenDA. These values were used into the model (Table 1).

Table 1. Principal tidal constituents for San Quintin Bay Lagoon

Harmonic	Amplitude	Phase
M2	0.485	124.792
S2	0.215	124.907
K1	0.308	203.348
O1	0.196	183.758
N2	0.116	250.2
K2	0.06	245.7
P1	0.104	84.2

Since the entrance to the bay is protected by a sand bar of 3 km long, the open boundary was selected to be far from the entrance to allow the tide to approach the lagoon in a natural way.

For the calibration reflection parameter alpha was tested, finding that the best performance is with a value of 1000 s^2

Water density was 1025 kg/m^3. The viscosity, diffusion, air density and acceleration of gravity values were 10 m^2/s, 1 m^2/s, 1 kg/m^3 and 9.81 m/s^2 respectively. While the condition in the walls of the channels was non-slip.

Bottom friction

The materials of the seabed of San Quintín Bay (SQB) and False Bay (FB) consist mainly of fine sand, very fine sand and silt; the fine silty sand having predominated. However, the same author found in a sediment sample, taken in front of El Molino Viejo, the proportion of 70% silt, 26% medium sand and 4% fine sand. Both in BSQ, and in the North portion of BF, the sediments are rich in

organic matter (IBAR et al., 2009).

For bottom roughness, the Chezy formula was used. Four types of bottom roughness can be determined (VAN RIJN, 1993): grain roughness (ks, grain); waveform- associated bottom roughness (ks, w); current-associated bottom roughness (ks, c) and apparent bottom roughness (ka).

For this work two areas were selected: the first one belongs to the main channels within the lagoon, which were indicated as predominately sandy bottom (ks) with a Chezy coefficient of 0.030 while for the second area (marsh areas), a Chezy coefficient of 0.070 was used.

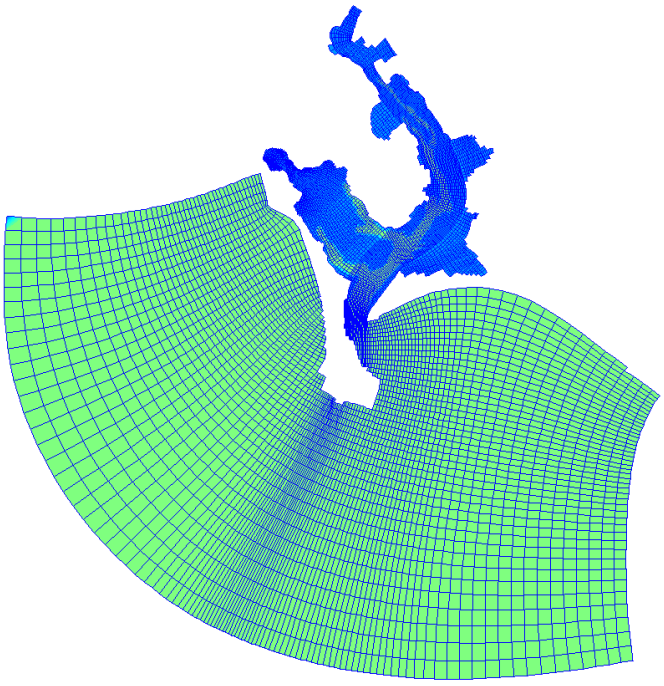

Figure 10. The green area indicates a sandy bottom area, whereas the blue one indicates a marsh (seagrass) bottom area.

In river flood plains and tidal plains, runoff resistance is determined by a combination of factors such as vegetation and bottom forms. Similar to other studies (LESSER et al., 2004; IGLESIAS; CARBALLO, 2009), the flow model was very sensitive to the wind drag coefficient and the bed roughness.

4.3. Model Calibration and sensitivity analysis

The tide can be divided into astronomical and meteorological, with the meteorological tide often defined as the difference between the observed tide and the astronomical tide (PUGH, 1987). To observed the influence of the meteorological tide in the model, was decided to calibrate and teste the model sensibility playing with 2 different scenarios:

a) Hydrodynamic Model 2DH with 7 tidal harmonics with constant wind field. The wind has been imposed to have constant direction (315^{o}) and intensity (3.15 m/s).

b) Hydrodynamic Model 2DH with 7 tidal harmonics and time-space variable wind filed

The main objective of the scenarios was to calibrate the model and to understand the sensibility of it, using winds, tidal harmonics and bottom roughness. Subsequently, once calibrated, to know the impact of the deepening in the planned area.

Because generally the tide varies with the moon phases (syzygy and quadrature), the simulation was performed for a period of 28/04/2004 07:00:00 – 13/06/2004 13:30:00, a total of 46 days, this in order to observe the monthly variations of the tide. The first 5 days of simulation where discarded since this period was used to let the model stabilized.

Before any calibration, the data was treated to remove the noise and outliers due to equipment error. The velocity field data had large offset and showed clear noise fluctuations around the tendency of the curve. In order to smooth the velocities field series, a moving average of 3 steps was applied to the *v* and *u* components of the velocity for each ADCP (Figure 11).

The Delft3D model was calibrated and tested for three different variables: water level (WL), vertical integrated currents (*u, v*), and residual vertical integrated

currents (|U|), three of them obtained from field measurements (ADCP's A, B and C).

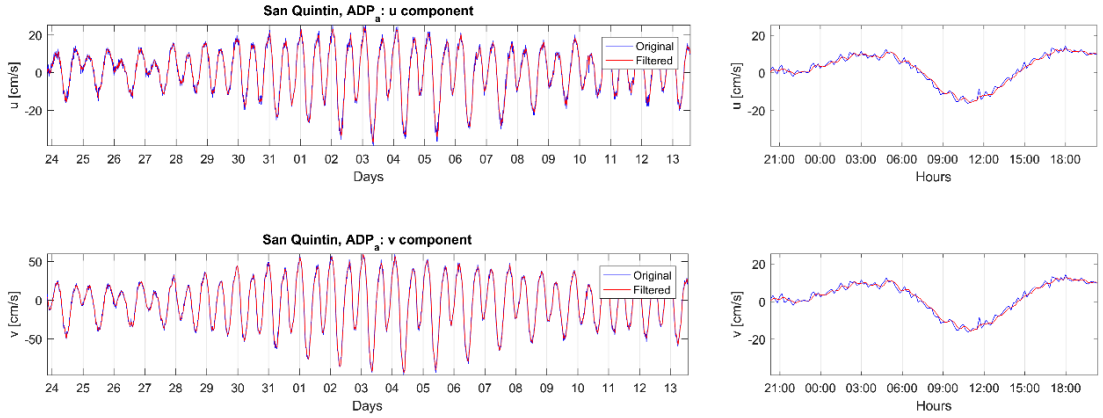

Figure 11. Example of the noise data treatment in ADCP position A

Comparisons between the measured and modeled series were performed based on the calculation of the following statistical parameters: Mean Absolute Error (MAE), Root Mean Square Error (RMSE) and the correlation coefficient (R^2). Mean absolute error (MAE) is not as widely used in the literature as RMS, although it is useful for identifying the mean difference between the estimated data and what is considered as a reference. The MAE is considered accurate and solid as a measure of ability of numerical models to reproduce (WILLMOT, 1982).

Comparing the MAE with another widely used statistic called BIAS, the BIAS does not provide information about individual errors and therefore cannot be used as a measure of simulation accuracy. Moreover, while providing an idea of the trend or systematic error, the bias is affected by the fact that positive and negative individual errors of the same magnitude cancel out in summation, which often leads to underestimation of simulation error. The MAE is less affected by points with anomalously extreme values or "outliers":

$$MAE = \left|\bar{d}\right| = \frac{1}{N}\sum_{i=1}^{N}|d_i| \qquad 19$$

where d_i is the difference between the simulated and the observed phenomena.

The closer $d_i = 0$, the better is the simulation (WILKS , 2006).

In addition to MAE, the RMSE is commonly used to express the numerical results with the advantage that RMSE presents error values in the same dimensions of the analyzed variable. The RMSE is defined by:

$$RMSE = [\frac{1}{N}\sum_{i=1}^{N}(d_S - d_O)^2 \qquad 20$$

Where d_S is the simulated data and d_o the observed one (WILLMOT, 1982).

The determination coefficient R^2 is the indicator that allows to know how well those results can be predicted. It represents the percentage of variation of the response variable that explains its relationship with one or more predictor variables. In general, the higher the R2, the better the fit of the model to the observed data.

4.4 Simulation of Dredging Activity

4.4.1. Scenarios and Dates of Simulation

Once the model has been calibrated, to identify the possible impacts of deepening in the north of the east arm area on the hydrodynamics, two numerical experiments were simulated:

- **(1)** identified as **Reference**, actual scenario without deepening activity in which the bathymetry used refers to a period previous to the port dredging project, based on measurements made in 2004 by the Oceanographic Research Institute (IIO); and
- **(2)** identified as **Deepened**, in which the bathymetry of the first experiment is changed to represent the intended quotas in the San Quintin Bay (east arm) dredging project,

covering a cycle of sicigia and quadrature. When performing the (2) scenario of interest, simulating a dredging in the northern area of the East Arm, the

bathymetry was modified and the model was shot from 28-April-2004 to 13-Jun-2004, (which corresponds to the period where all instruments measured simultaneously). The surface of the polygon area to be deepened by dredging is 116,221 m^2, and a volume of 2,752.75m^3, with an average dredging depth of 2 m (Figure 10).

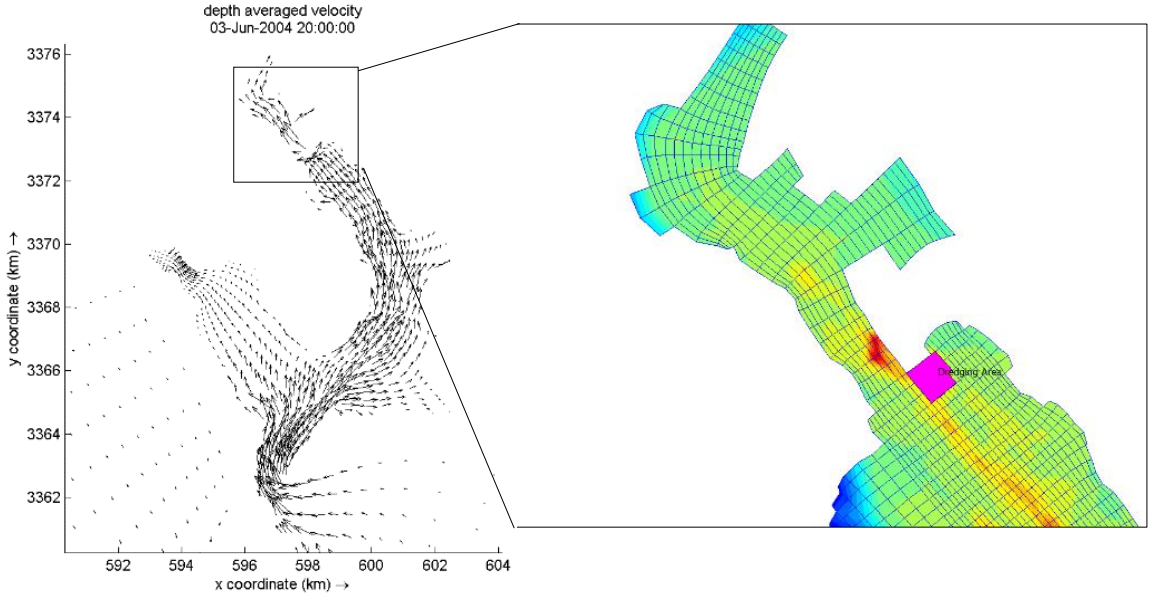

Figure 12. Marked within a box is the area of interest in which dredging will take place (pink area in the right).

To clarify and summarize the scenarios used in the development of this work, Table 2 summarizes its use and description of each of them.

Table 2. Summary of scenarios used for calibration and simulations

Scenario	Description	Section
a	Hydrodynamic Model with constant wind field: direction (315º) and intensity (3.15 m/s).	Calibration
b	Hydrodynamic Model with variable wind field	Calibration
1+b	Reference: actual scenario using variable wind field (scenario b), without deepening	Simulation of Deepening
2+b	Deepened: scenario with a deepened polygon, using variable wind field (scenario b), in the east arm	Simulation of Deepening

4.4.2. Hydrodynamic changes analysis

To analyze the hydrodynamic changes between **(1)** and **(2),** the time series for water elevations and velocity were compared. For the velocity, both components as well as the magnitude were subtracted: scenario **(2)** – scenario **(1)** (*u* component velocity, *v* component velocity and magnitude of the velocities). For each component of the velocity an analysis was made:

$$u' = u_{ii} - u_i \qquad 21$$

$$v' = v_{ii} - v_i \qquad 22$$

$$V = \sqrt{u'^2 + v'^2} \qquad 23$$

Where u' and v' are the difference between both scenarios (1 and 2), and V is the magnitude of the differences.

4.5. Monitoring points

In order to monitor the model performance, as well as the calibration accomplishment three point where set in the positions where the three ADCP's were placed for data collection: A, B and C. Also, one more monitoring point was placed in the polygon where the dredging activity will take place: D.

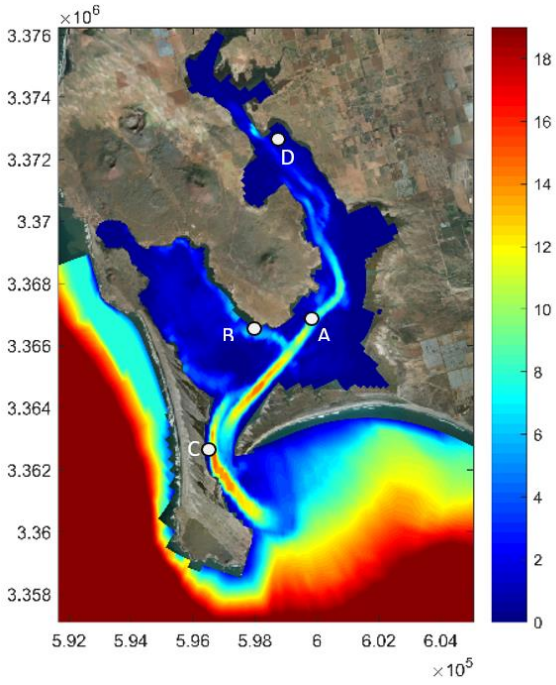

Figure 13. Monitoring Points stetted in the model

The three points A, B and C were used to calibrate the model, while point D was the one used to compare both scenarios: reference and dredged.
The time series obtained for water elevation and currents for both scenarios (Reference and Deepened) in point D were compared.

4.5.1. Time series Analysis

The Delft3D-FLOW model generates the time series for the currents according to the geographical North of the place, which implies that the main channel (where the highest currents are located), is not aligned with the geographical North, presenting an approximate difference of 35°(θ). In the Figure 14, the difference between the main axis of the channel and the geographical North is better visualized.

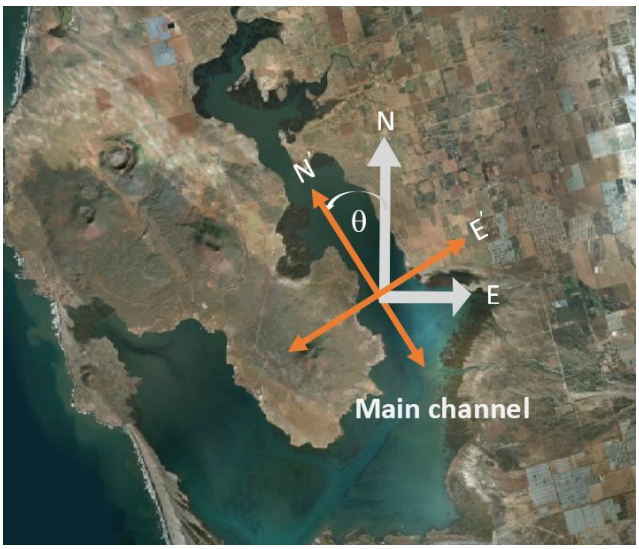

Figure 14. New reference frame alienated to the main channel

In order to obtain a better hydrodynamic analysis, the time series for velocity were aligning to a new “referential framework”, where the new "north" is aligned with the main axis of the channel.

5. RESULTS AND DISCUSSION

5.1. Calibration

5.1.1 Water Elevation Calibration

In section *4.3. Model Calibration and sensitivity analysis*, two scenarios were set (*a* and *b*) for calibration, the first one with astronomical tide and constant wind field, and the second one with astronomical tide and time-space variable wind field. For the previous mentioned scenarios, the Root Mean Square Error (RMSE), Mean Absolute Error (MAE) and the correlation coefficient (R^2) were the statistical parameters used to evaluate the model performance. The results for water elevation time series for the three ADCP's for scenarios *a* and *b* are shown in the following table:

*Table 3. Statistical parameters obtained for water elevation comparing observed (ADCP) and simulated time series for scenarios **a** and **b** during calibration.*

ADCP	Scenario *a*			Scenario *b*		
	RMSE (m)	MAE (m)	R^2	RMSE (m)	MAE (m)	R^2
A	0.115	0.891	0.948	0.104	0.085	0.959
B	0.098	0.0782	0.965	0.104	0.084	0.961
C	0.112	0.871	0.911	0.112	0.091	0.952

The best performance of the model was obtained for the second scenario: *b,* when time-space variable wind field was applied (meteorological plus astronomical tide).

For water elevation scenario *b* (Figure 15) the model results match the trend and dynamics of the observed data. The model presented a high correlation with

measured data in both scenarios, however, for scenario *b* the R^2 showed a slightly higher value.

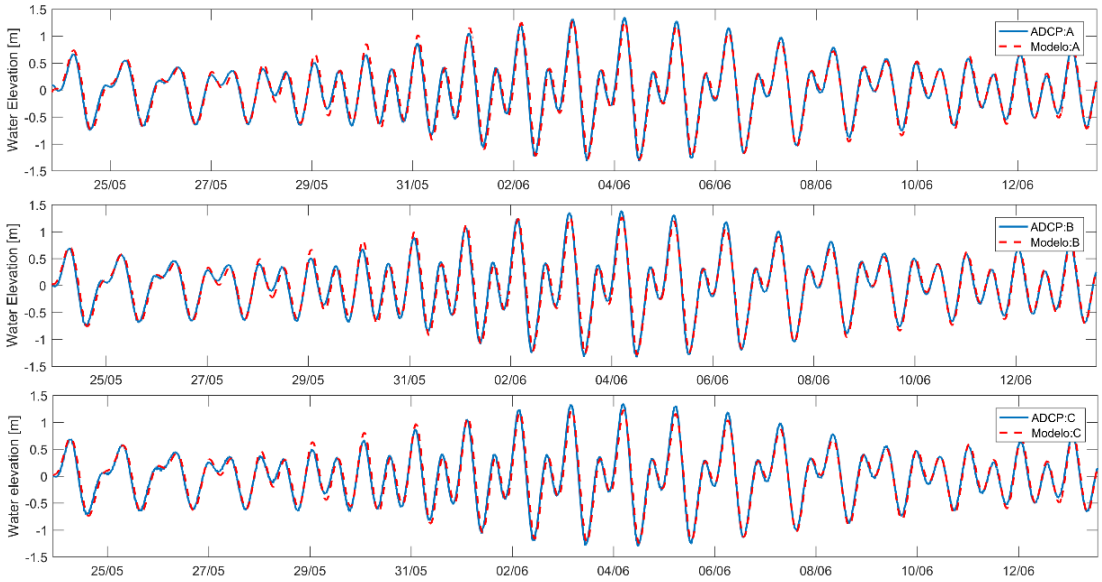

Figure 15. Water elevation comparison between ADCP time series and the model results for Scenario b.

In the following sequence of images, the transition between high tide and low tide (ebbing) in the coastal lagoon for scenario *b* was simulated:

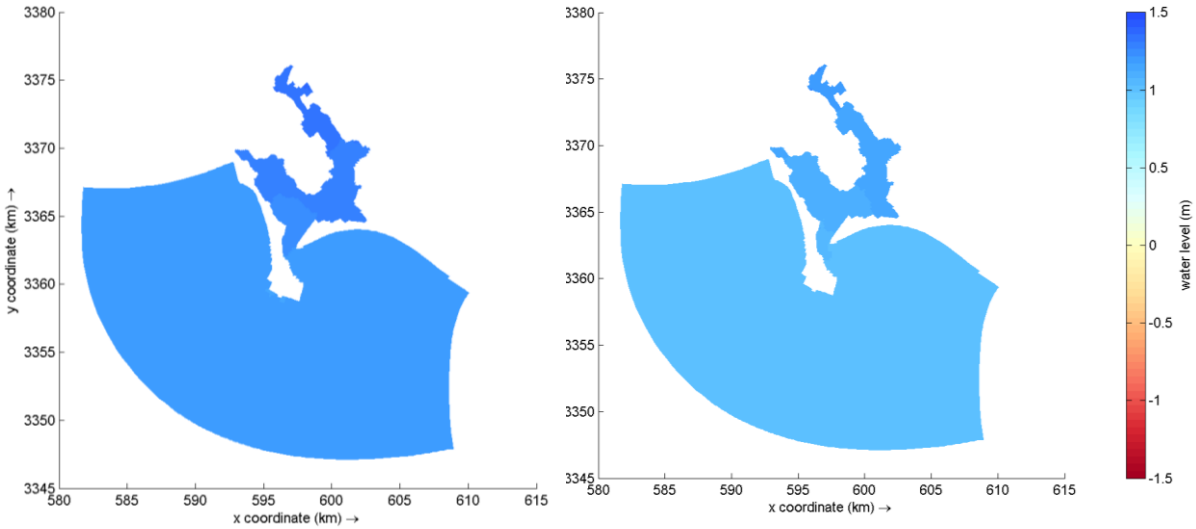

a) 04/06/2004 05:00:00 *b) 04/06/2004 06:00:00*

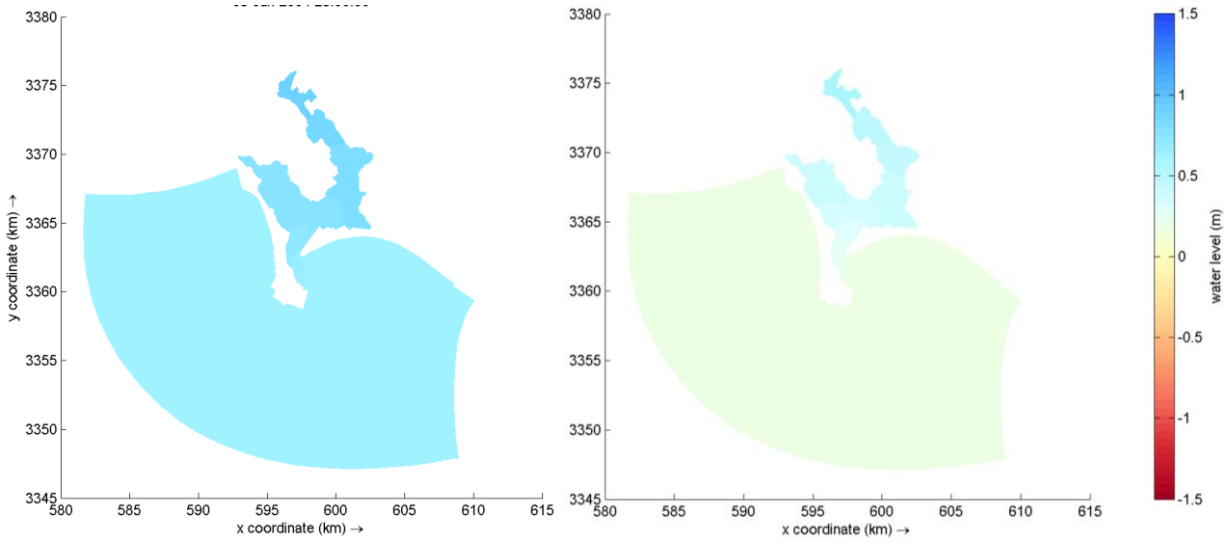

c) 04/06/2004 07:00:00 *d) 04/06/2004 08:00:00*

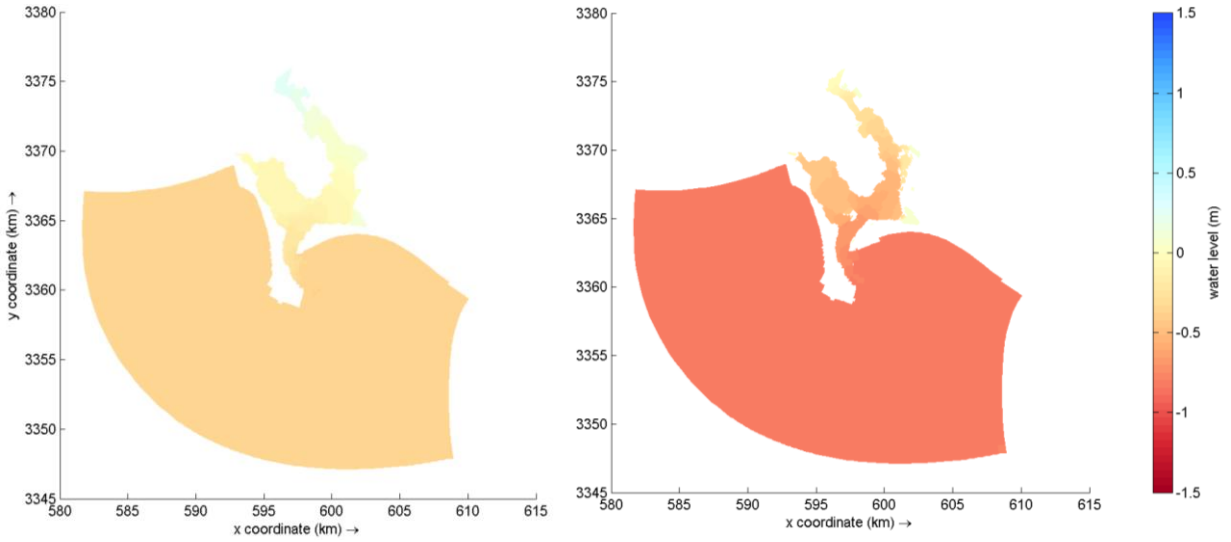

e) 04/06/2004 09:00:00 *f) 04/06/2004 10:00:00*

Figure 16. Series of images showing the behavior of the water level, with a difference of one hour between each image.

Figure 16a - 16f, shows that the model was capable of reproducing the dynamics for Water Level. A comparison between Figure 16 and Figure 15 indicates that

the model reproduced with high correlation the tidal range (2.75 m for the chosen simulated data in Figure 16) for ebbing during spring.

Examination of sea-level records shows that the interval from low to high water is shorter than the interval from high to low water: the rise time is more rapid than the fall.

5.1.2. Velocities Calibration

For the depth-averaged velocities, the ADCP-B was discarded since its location (area between the two arms with a lot of turbulence and in a very shallow zone) generated inconsistency in the measured velocity time series. Although the time series obtained through the ADCP-B for sea level did not show great inconsistencies, the measured data for the velocities were not reliable.

Based on the performance of the model during sea level calibration, and because in previous researches wind was found to be the secondary main forcing agent (after the astronomical tide) in the dynamics of the bay, the calculated statistical parameters for depth averaged velocity were based on scenario *b* (astronomical tide plus time-space variable wind field). A visual analysis (Figure 17) shows that for ADCP-A, the *u* and *v* components underestimated the velocities, mainly during spring tides, while during neap tides the underestimation reduces.

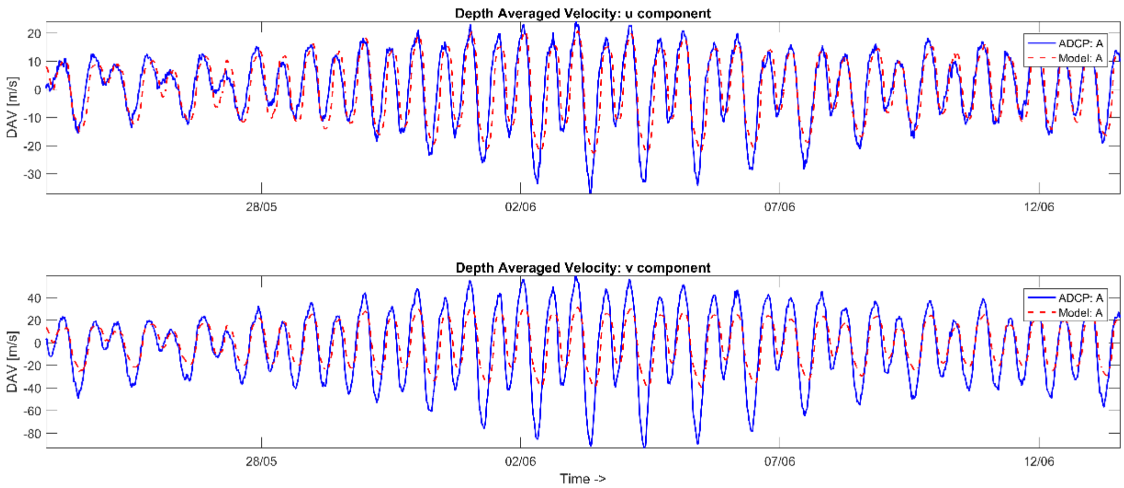

Figure 17. Depth Averaged Velocity comparison between measured data (blue) and simulated data (red) for u and v components for point A

For observed time series, *u* and *v* component showed averaged velocities of 10.15 cm/s and 26.3 cm/s while for simulated time series the averaged velocities where 10.34 cm/s for *u* and 16.88 cm/s for *v*.

When comparing averaged *u* component, the velocity averaged does not show a great difference, even showing that the model velocity is slightly higher, but a graphic analysis (Figure 17) helps to understand that the model underestimates the velocities during spring tides while during the neap tides the difference is minimum.

For both components in ADCP-A, the greatest variation between time series belong to a spring tide (01/06/2004 to 04/06/2004), with an averaged underestimation of 8 cm/s for *u* component and 20.5 cm/s for *v* component.

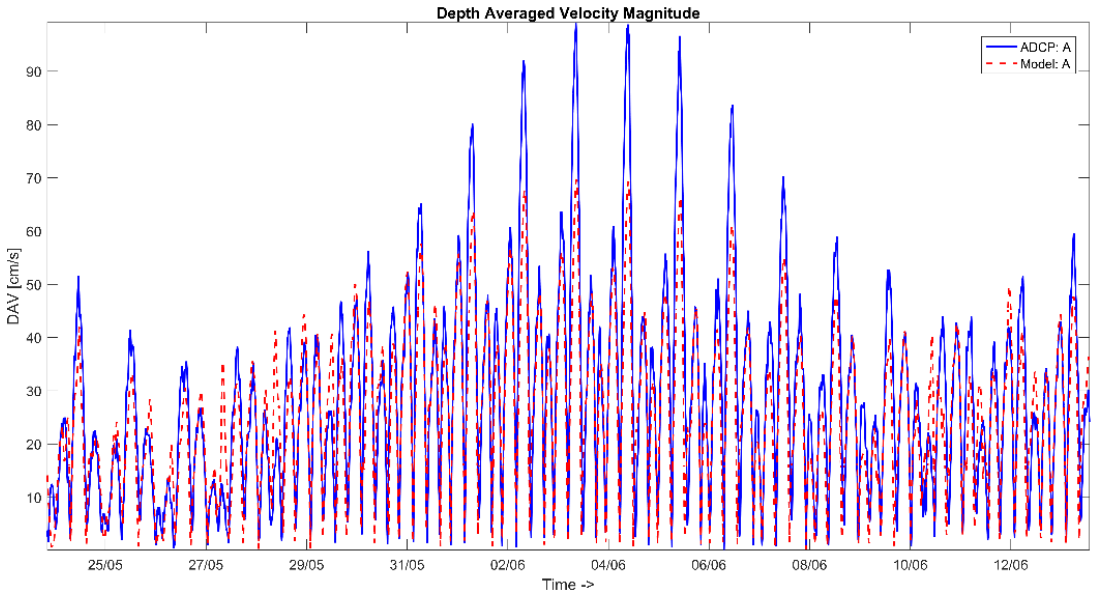

It is believed that the model underestimated the currents due to the chosen bottom roughness coefficients, with greater atrium in the shallowest areas.

The increase in roughness and the blockage of water flow due to vegetation is an important factor influencing the flow velocities. This causes a notable characteristic of the hydrodynamics: the asymmetry between ebb and flood

currents.

Regarding the magnitude of the velocity for the ADCP-A (Figure 18), the model presented an underestimation of the magnitude, mainly in peak values where the currents registered a 25 cm/s averaged underestimation. A 3D model carried out by Delgado Gonzales et al. (2012), showed an underestimation of the magnitude of 1 cm/s at maximum values. He also reported a correlation coefficient R^2 of 0.87.

In Figure 17 and Figure 18 the velocities scale for *v*, when comparing to velocity scale of *u,* is approximately twice the values of *u* component, showing that the dominant component is *v*.

A visual comparison between simulated and observed time for velocity series for the ADCP-C is observed in Figure 19 and Figure 20.

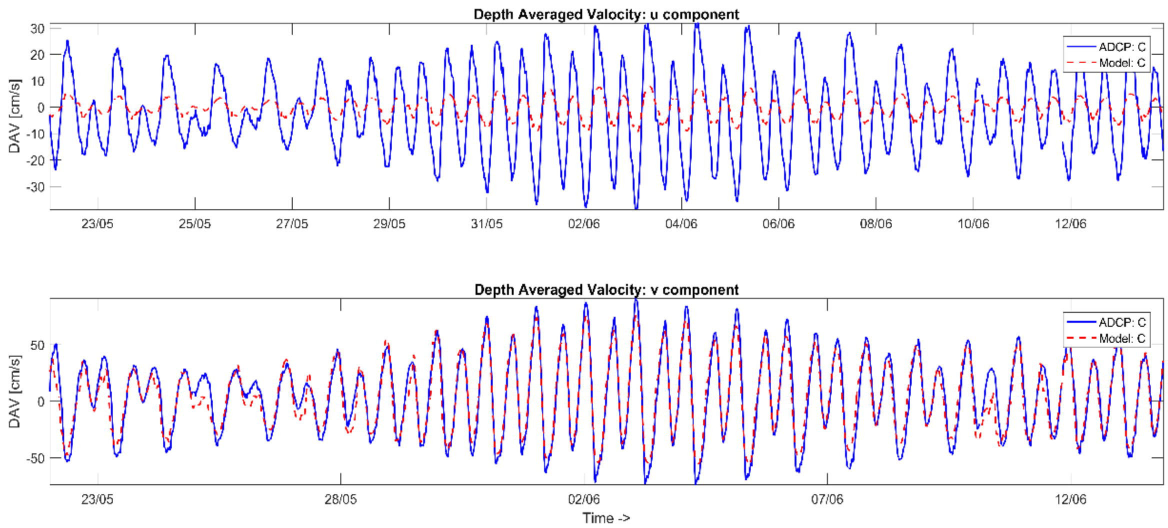

Figure 19. Depth Averaged Velocity comparison between measured data (blue) and simulated data (red) for u and v components for point C.

As happened for ADCP-A, the ADCP-C underestimated the velocities for both components. The averaged velocities for simulated time series were 3.0 cm/s for *u* component and 28 cm/s for *v* component, while for the observed time series were 13.6 cm/s for *u* and 30.25 cm/s for *v*.

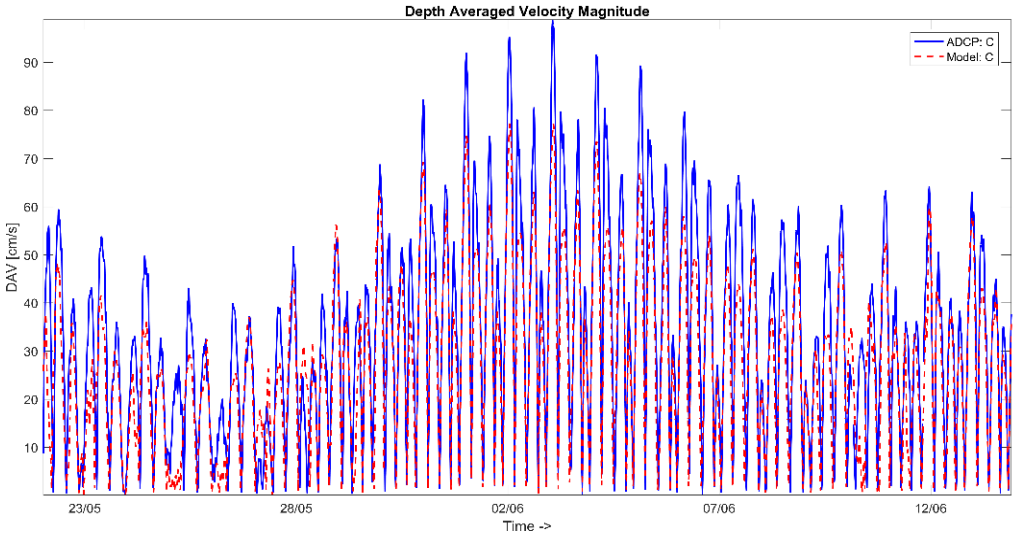

Figure 20. Depth Averaged Velocity Magnitude comparison between measured data (blue) and simulated data (red) for C point.

Although *u* presented a 76.5% (10 cm/s) underestimation for the simulated series, this is small taking into account that the dominant component is *v*, which presented an underestimation of just 7.4% when comparing simulated and observed time series (1.8 cm/s averaged difference).

Table 4. Calibration statistical parameters for Depth Averaged Velocity

ADCP	Scenario *b*								
	RMSE (cm/s)			MAE (cm/s)			R^2		
	u	v	|U|	u	v	|U|	u	v	|U|
A	5.228	16.186	15.352	3.973	12.491	11.488	0.816	0.850	0.600
C	12.405	10.167	10.665	10.580	8.143	8.681	0.940	0.918	0.800

Table 4 shows an overview of the resume of statistical parameters for the ADCP-A and ADCP-C. The RMSE, MAE and R^2 were calculated for the *u* and *v* components and for the velocity magnitude of the time series (not the magnitude of the errors for u and v, but for the differences of the magnitude). For both ADCP´s high values of R^2 were obtained (between 0.8 and 0.94).

It is verified that the greatest differences, indicated by the MAE, are for the ADCP-C. When comparing the statistical results for the velocity components between ADCP-A and ADCP-C, the ADCP-A appear to fit better since the errors have lower values, but actually, this is because the velocities range in ADCP-C is higher than in ADCP-A. The velocities range for ADCP-A varies 55 cm/s for *u* component and 130 cm/s for *v* component, while for ADCP-C varies 70 cm/s for *u* and 170 cm/s for *v*.

ADCP-C is located in the mouth of the SQBL, where the higher currents are present, while ADCP-A is located in the east arm (SQB), close to the main and deeper channel, where velocities are considerably lower than those registered in the mouth.

In general, the simulations satisfactorily represented the local elevation and current pattern, as indicated for R^2 with values of about 0.95 for elevation and 0.80 for currents.

To understand the hydrodynamics of the lagoon, two moments where chosen for the monitoring point **"A"**:

a) Maximum velocity during syzygy
b) Maximum velocity during quadrature

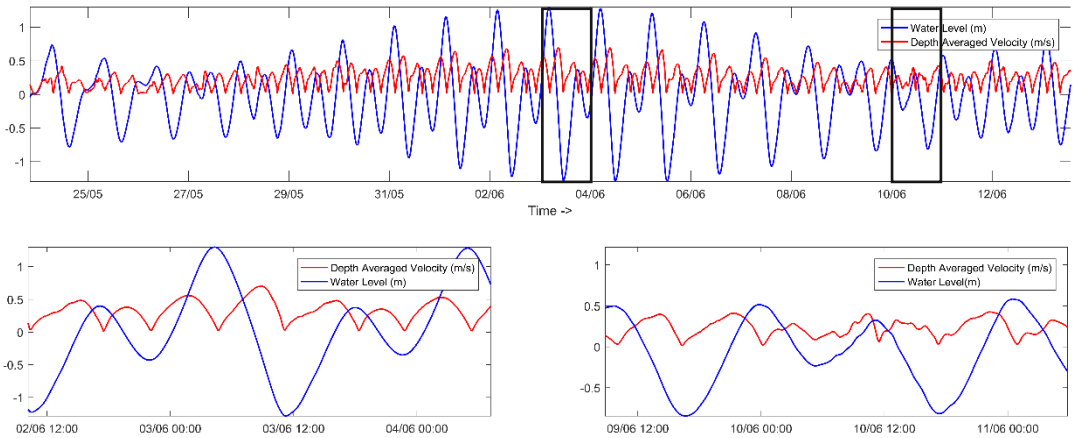

Figure 21. Comparison between Water Level and Depth Averaged Velocities for syzygy and quadrature.

The two dates when maximum currents during syzygy and quadrature occurred were:

- Ebbing in spring tide, maximum current value: June 3th, 0.6970 m/s
- Flooding in neap tide, maximum current value: June 10th, 0.4261 m/s

The current values for spring tide were 63% higher than those for neap tide. In general, it was found that the values for ebb current were higher than those for flood current. It is believed that during spring tides, following low water the water level rises, but there is then a slackening of the tidal stream and a water level stand for a further half and an hour before the final rapid rise to high water, over the next two- three hours. The effect is known locally as the 'young flood stand' (PUGH, 1987).

The flood and the double high water last approximately nine hours, leaving only 3.5 hours for the tidal ebb, which is therefore associated with very strong ebb currents, and second, that the large marshes areas of the lagoon have an impact on the lower magnitude currents during flooding tide.

In Figure 23 and Figure 24, vectors and water elevations are plotted for ebbing (spring tide) and flooding (neap tide).

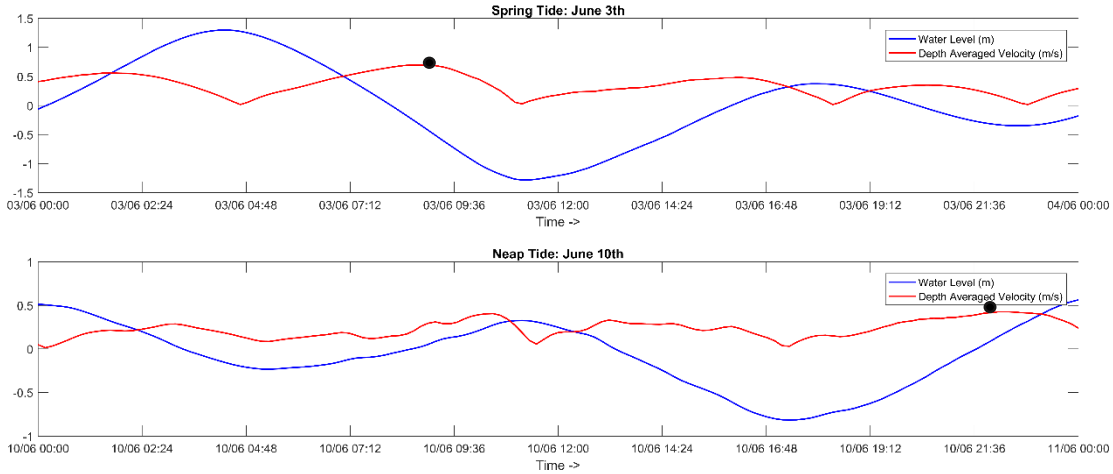

At the estuarine mouth, the flow follows the main channel and then forms a fan shaped flow field with the strongest currents observed at the southern section of the estuary entrance.

As the tide changes, water starts to propagate inwards mainly through the west section of the mouth. Inside the lagoon, the flow propagates mainly through the deeper channels. The highest values are attained along the navigation channel, in particular, in the central portion of the constriction. The Maximum Flood (MF) current at the mouth attains values close to 1.1 m/s, while for Maximum Ebb (ME) was close to 0.80 m/s (during spring tides).

The dynamics of the lagoon varies from the mouth to the north of the arms: in the mouth and main channel close to the entrance the velocities can rich a value of 1.1 m/s, while the arms and going towards north, these values decreases.

Spring tides are associated with higher current velocities in the main channels. While the maximum currents happened, the sea level is close to zero. This behavior this behavior resembles the theory that describes a standing wave. The results obtained for the simulated velocities time series were close to those reported by Juárez (2014), who reported the maximum currents in the mouth of the lagoon, with values just above the 100 cm/s and lower velocities in the main channels of the lagoon, with a variation between 35 cm/s and 70 cm/s .

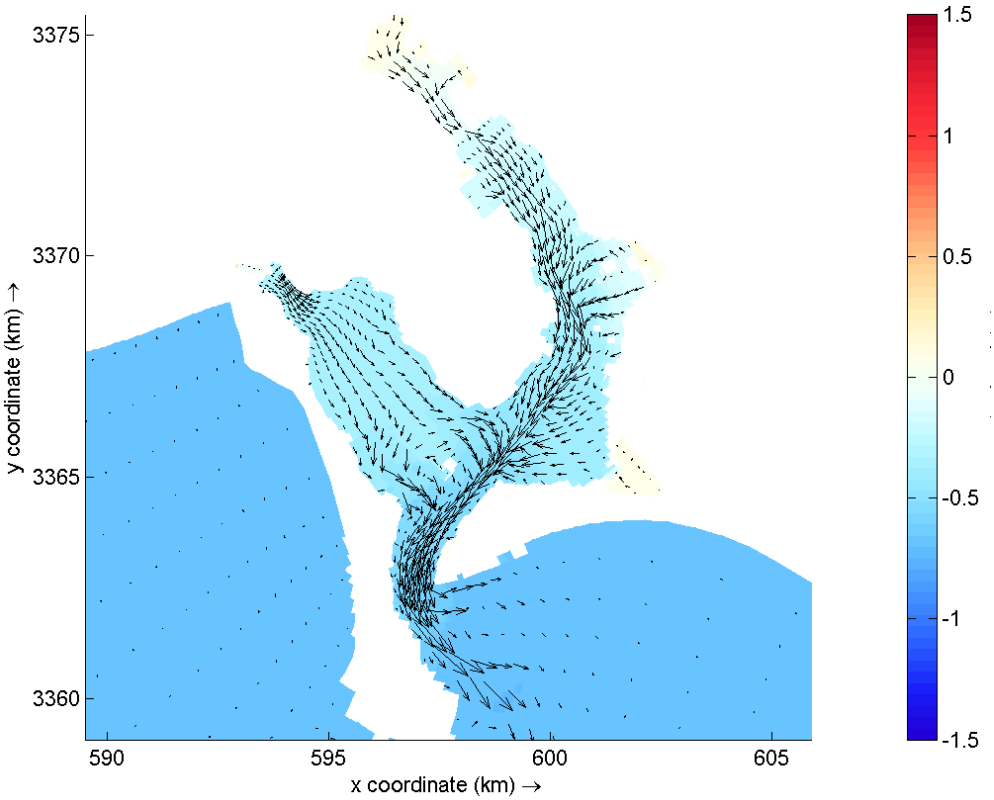

Figure 23. The vectors shows the velocity field and the colormap represents the water elevations for ebbing during spring tide

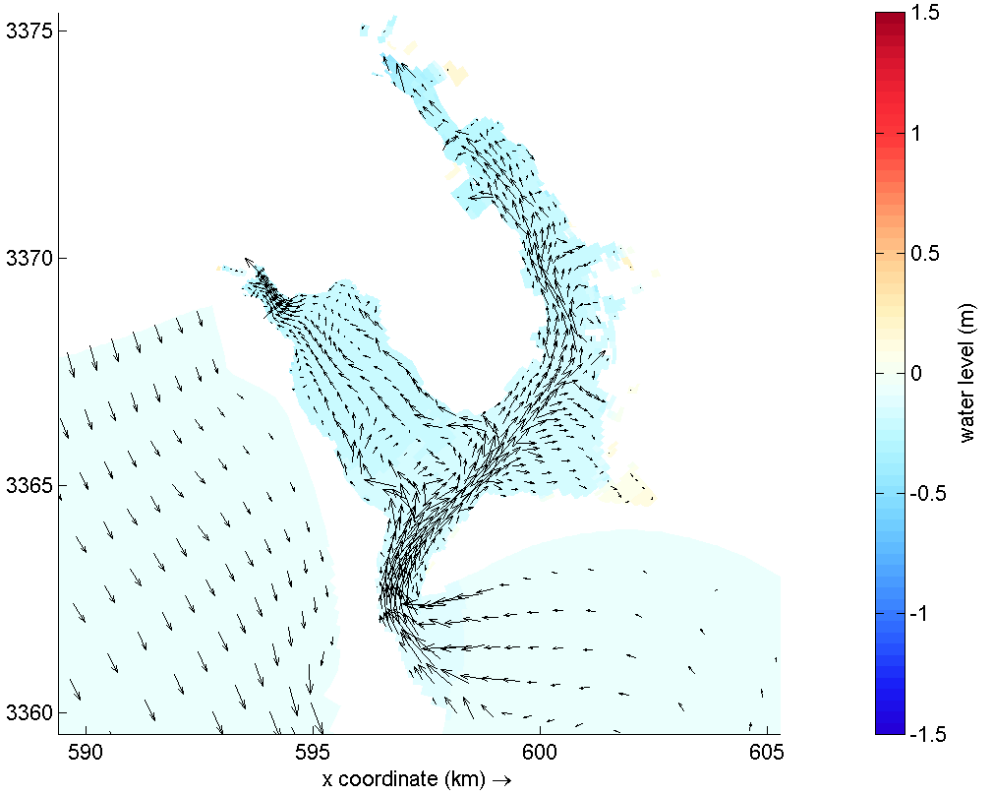

Figure 24. The vectors shows the velocity field and the colormap represents the water elevations for flooding during neap tide

5.2. Simulation of Hydrodynamics after Deepening

5.2.1. Hydrodynamics: water level

The time series for the water level oscillation were simulated for a period of 47 days, this with the intention of observing the behavior of hydrodynamics during spring and neap tides. The first 5 days of the time series were disregard to give the model a stabilization time.

The elevation series obtained for the Reference (1) and Deepened (2) experiments were compared at point "D" in order to analyze the impact of the deepening in the north of the eastern arm of the lagoon.

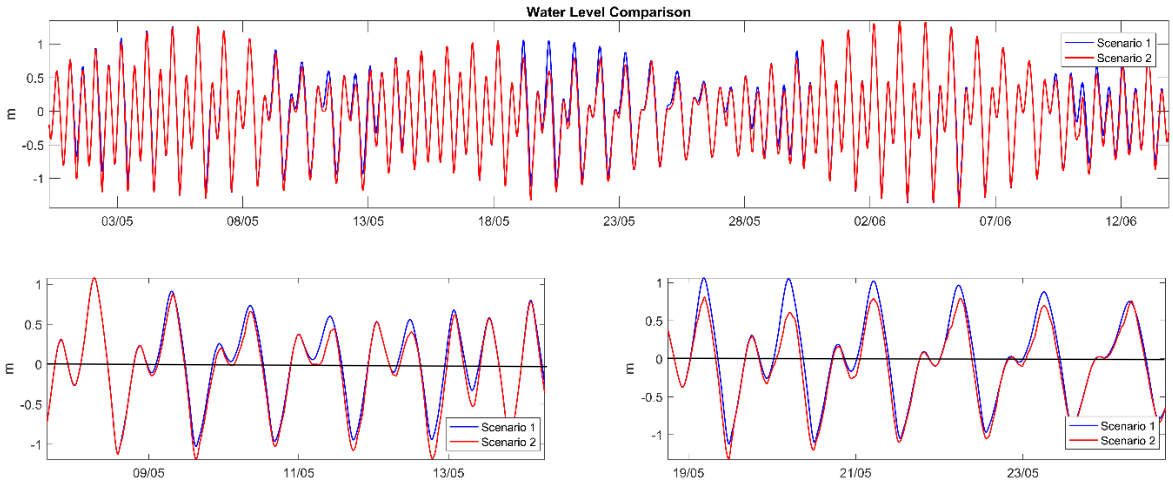

Figure 25. Water Level Comparison between reference and dredged scenarios

From a visual comparison, it is possible (but hard), to perceive small differences between the water level time series for the two experiments (Figure 25). The differences between the two scenarios presented a pattern: for the scenario (1) the amplitudes that were greater than those of the scenario (2) are presented in the high tide, while for the scenario (2), the times when the amplitudes are higher than the scenario (1) is at low tide.

From the Figure above, two periods with the greatest differences are easily identified: the first period goes from 09/05 up to 13/05, and the second one from 19/05 until 24/05. The first period belongs to a neap tide while the second to a

spring tide.

To get a better understanding, the differences between the Reference scenario and the Dredged scenario are shown in the following graph (Figure 26). In this time series, a subtraction of (2) - (1) was performed.

The results shows that, in general, the elevation for the dredged stage decreased by 0.0485 m on average, that is, after dredging the sea elevation presented approximately 4 cm less (averaged) tidal ranged when compared to the Reference scenario.

Based on Figure 25, a phase difference can be observed, with the red line under the blue one, generally in syzygy. If a horizontal line (elevation = 0) is considered, the red line (time series for deepened scenario) arrives before the blue one (time series for reference scenario), which means that the red one moves faster than the blue one.

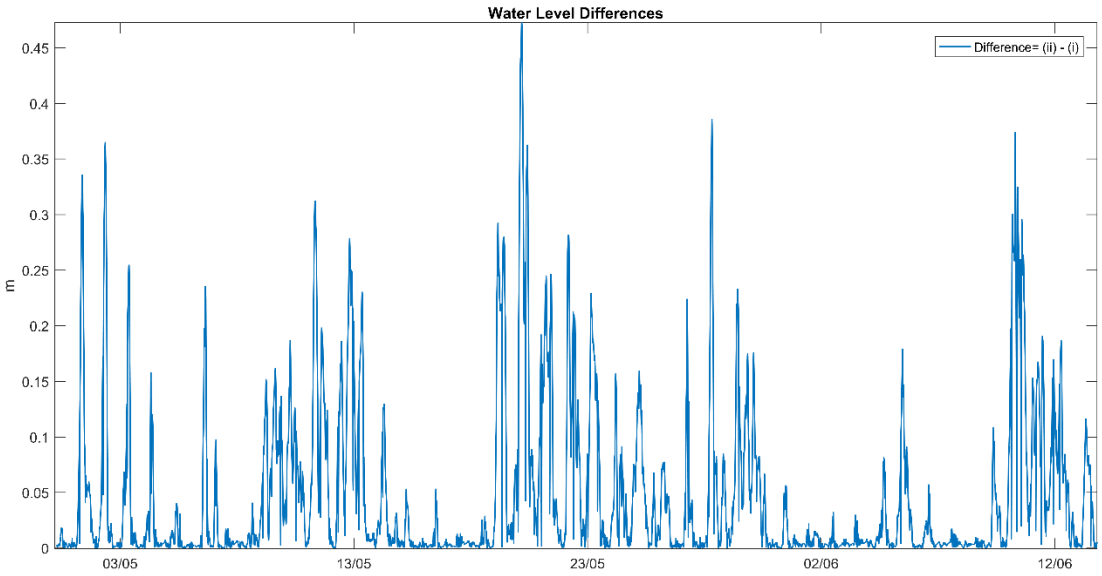

Figure 26. Difference in water elevation time series between the non-dredged and dredged scenario

The difference obtained between one scenario and another was in the order of centimeters. A peak value was also observed, in which the difference between both scenarios was 47 cm (a decreased of 47 cm was recorded during a spring tide). In general, the deepened scenario presented a decrease in water elevation of 15% during spring tides.

To better evaluate the differences between the results obtained from the two experiments, the series were compared based on the MAE, with the reference values being the values corresponding to scenario 1.

The MAE value obtained for “D” point was 0.0507 m. The previous result was expected, based on the energy conservation: the decrease in the depth of the sea causes an increase in the amplitude of the tidal wave. If the energy flux is to remain constant as the water depth increases, the wave amplitude must decrease (PUGH, D.,1987).

5.2.2. Hydrodynamics: depth averaged velocity

To analyze the impact in the local hydrodynamics simulating a deepening by dredging activity, (without taking into account the sedimentation transport or water quality), in the northern area of the eastern arm, current data obtained from the model monitoring point "D", were used.

The time series for the velocity were simulated for a period from 28-04 until 13-06 and the first 5 days of the time series were disregard to give the model a stabilization time.

The velocities were adjusted to a new referential framework. The intention was to allow a better analysis of the dominant component of the currents and of the studied area. In Figure 27 and Figure 28, the velocity components (*u* and *v*) are observed for both scenarios.

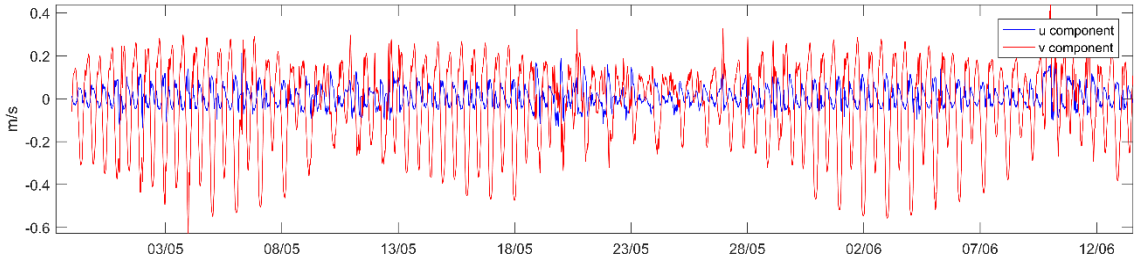

Figure 27. Velocity components u and v with the new frame of reference for scenario 1(Reference)

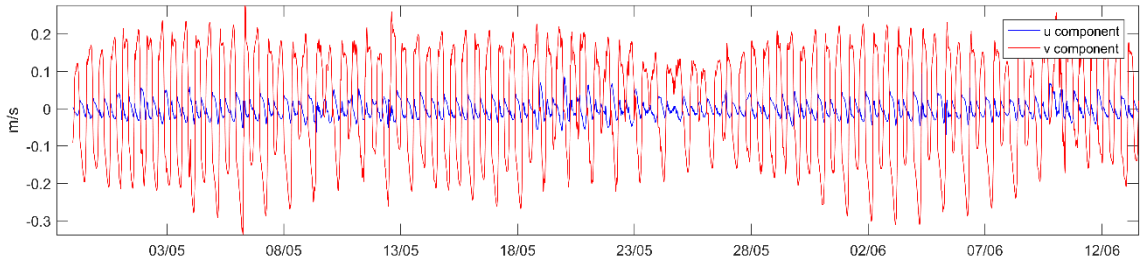

Figure 28. Velocity components u and v with the new frame of reference for scenario 2 (Deepened)

It can be appreciated that the adjustment to the new frame of reference worked properly, since the component *u* maintains values close to zero, while component *v* manifests itself as the predominant one. In scenario (1) (Figure 27), component *v* varies from zero to 0.6 m / s for ebbing currents and from zero to 0.3 m / s for flooding currents, which shows greater currents for ebbing.

For the second scenario the velocities range for flooding currents presented values close to scenario one, varying from zero to 0.3 m/s, while for ebbing currents a notable reduction in the velocity can be seen.

To go deeper into the hydrodynamic changes analysis, first, a comparison between the components of the velocity (*u* and *v*) for the scenario (1) and scenario (2) was performed (Figure 29 and Figure 30).

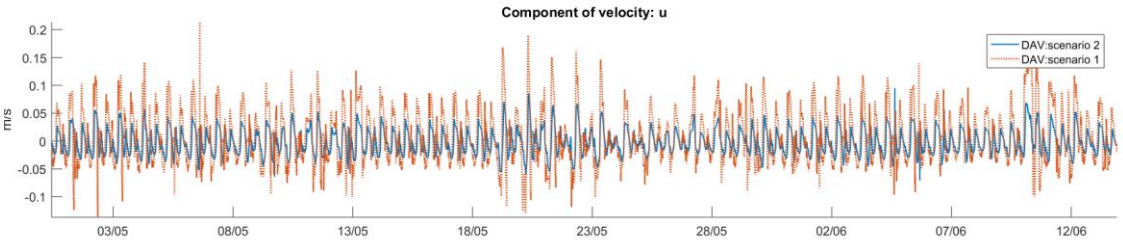

Figure 29. Depth Averaged Velocity comparison between scenarios (1) and (2) for u component

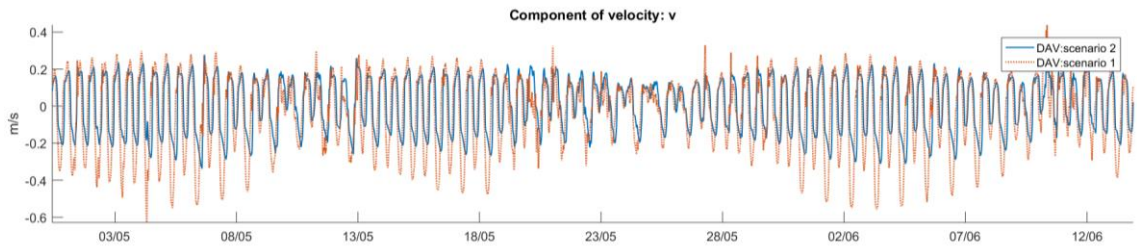

Figure 30. Depth Averaged Velocity comparison between scenarios (1) and (2) for v component.

In figure 30 it's interesting to remark that the initial asymmetry showed for the Reference scenario reduces after the deepening simulation for both components. In the Reference scenario, a tidal asymmetry with ebbing dominance is evident, while for Deepened scenario this asymmetry is evidently affected, reducing the ebbing dominance.

For the *u* component of the velocity, a time offset between the time series was not recorded (Figure 29 and Figure 30), however, in the *v* dominant component an offset appears between the scenario one and the scenario two: the deepened scenario presents an offset of approximately 0.5 hours ahead.

To verify the time lag between the two time series for *v* component, two new monitoring points were added to the model. The first one was located northern to the deepened area "E", and the second one "F", southern (Figure 31).

When comparing the time series for scenario 1 (Reference) and 2 (Deepened) in this new two points, it was determined that there was no time lag, which means the only area that presented the 0.5 hours lag was the point in the affected area, "D".

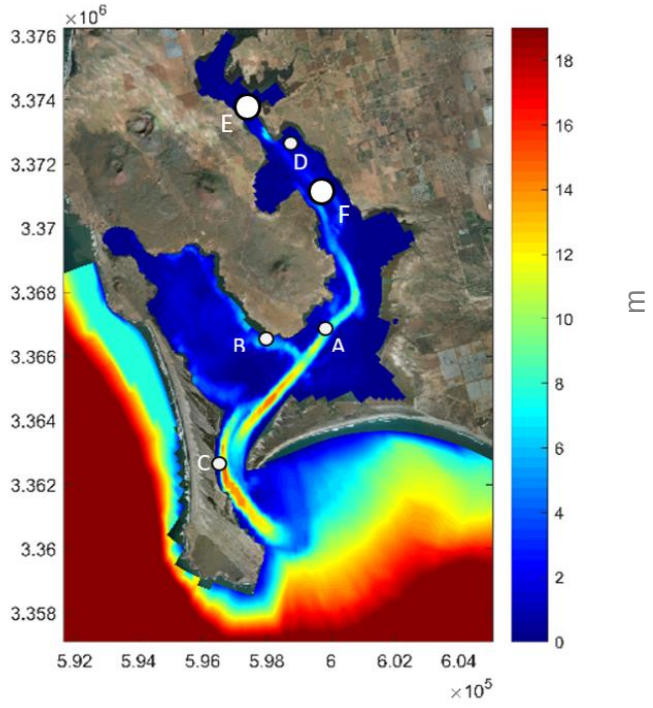

Figure 31. Location of monitoring points in the model: adding two new points "E" and "F".

Returning to the analysis at point D, where is the comparison between the Reference and Deepened scenario, the greatest differences between the two scenarios occurred during periods of syzygy, while during quadrature the currents maintained a very close behavior between both scenarios.

Both components of the velocity decreased for scenario (2). To make it more evident the equations 21 and 22 were used:

$$u' = u_2 - u_1 \qquad 21$$

$$v' = v_2 - v_1 \qquad 22$$

In Figure 32 these two equations are plotted for point D.

In reference to the moments when the maximum currents occurred, the maximum value for u_1 (Reference scenario) was 0.2490 m/s while for scenario 2 (Deepened scenario) u_2 was 0.0951 m/s. This means that for critical values (maximum velocity), the scenario two is 0.154 m/s (60%) less intense than scenario one.

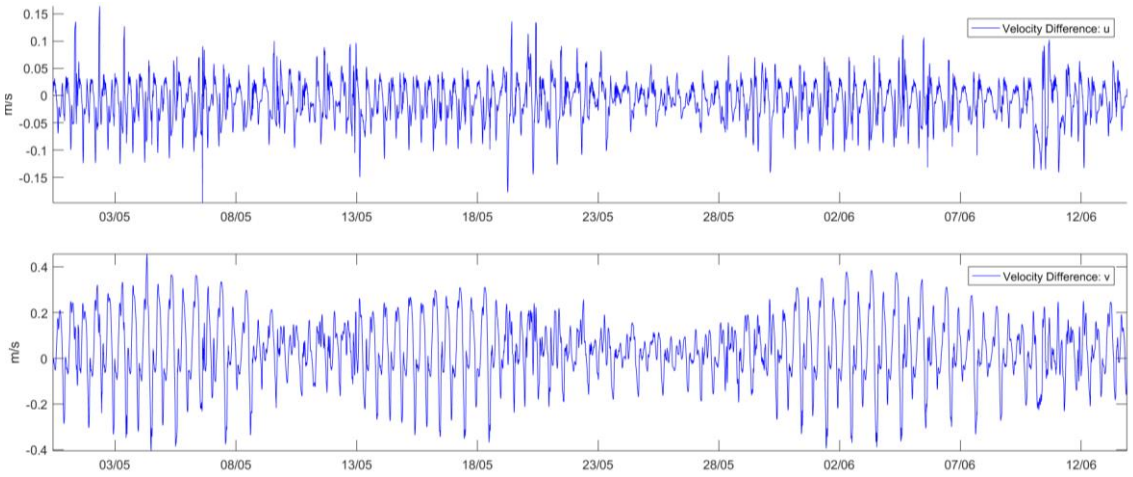

Figure 32. u' and v' time series

For *v* component, the maximum velocity recorded for scenario one v_1 was 0.4418 m/s while for the second scenario the maximum value recorded v_2 was 0.2767 m/s, this is 0.1651 m/s (38%) less than v_1.

The MAE was used to estimate the difference between both scenarios. For u component the MAE was 0.0296 m/s while for *v* was 0.1137m/s. The results of the "D" point indicates that in the region where the bathymetry was deepened, there was a decreased in both flood and ebb currents and throughout the whole quadrature/sizygy cycle.

In environmental applications, a reduction in the currents can directly impact residence times and renewal of water bodies, especially in a location far from the mouth (ocean connection) as is the studied area in here, compromising water quality. Being a site surrounded by agricultural areas, and exponential human development, this area is exposed to organic and inorganic wastes that can cause nutrient enrichment and even eutrophication in semi-confined areas or with little water renewal.

To see the total changes in the magnitude, the equation 23, that relates the differences between the two scenarios, was used. The difference of the magnitudes for scenario (1) and (2) is ploted below (Figure 33) based on:

$$V = \sqrt{u'^2 + v'^2} \qquad 23$$

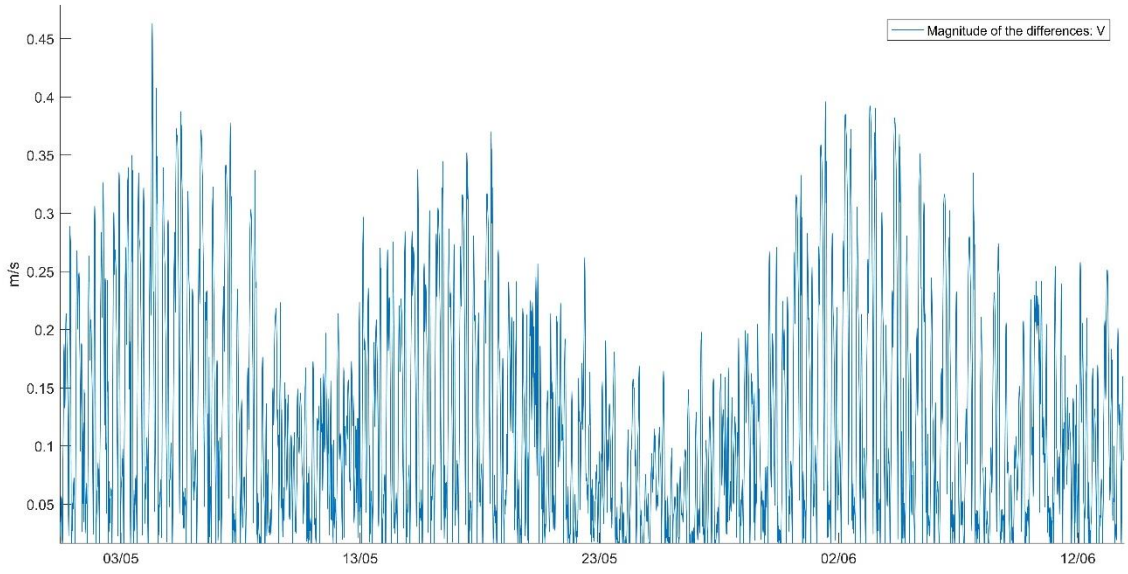

Figure 33. Total magnitude differences (decreased) between scenario (2) and scenario (1) for "D" point

Figure 33 shows the total change in the magnitude: the decrease in the magnitude of the velocity that was obtained when comparing scenario 1 and scenario 2. Figure 33 confirmed that the velocities for the original scenario without bathymetric modifications show higher velocities than the deepened simulation. Figure 34 is used to get a better understanding of the values of Figure 33.

It is interesting to highlight the greatest peak of maximum difference: it shows a difference (decrease) of 0.4632 m/s for May 4, when the maximum high tide is found during spring tide cycle. That is, the velocity decreases approximately 70% for an extreme scenario.

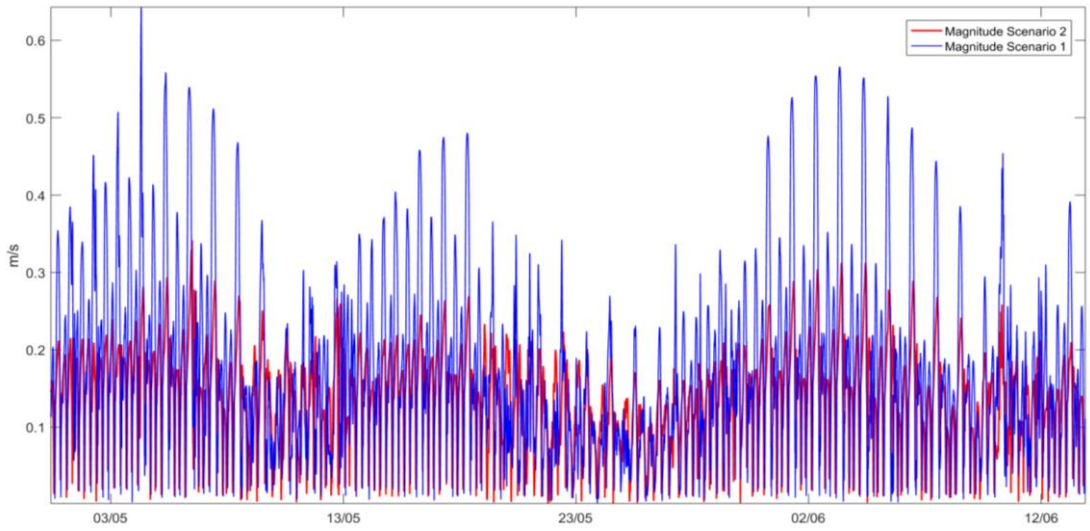

Figure 34. Depth averaged velocity magnitude for scenario one (blue) and scenario (2) for "D" point

In Figure 34, the greatest differences can be identified in three specific periods: the first one from May 3 to 7 with an averaged decreased of 0.1583 m/s, the second from May 14 to 21 with an averaged decreased of 0.1334 m/s, and the third from May 28 to June 4 with an averaged decreased of 0.1417 m/s. The three previous moments corresponded to periods of syzygy.

Based on the above, it can be concluded that the mayor changes due to deepening activity will be seen during spring tides, where the currents will register a decreased of 0.14 m/s averaged. The MAE for the magnitude was 0.0931 m/s. The total changes estimated trough the MAE parameter are summarized in the

following table:

Table 5. Mean Absolute Error between the reference and deepened scenarios.

Parameter	MAE
Water Level	0.0507 m
u component	0.0296 m/s
v component	0.1137 m/s
Magnitude total change	0.0931 m/s

This result makes physical sense based on the law of mass conservation, where the mass that enters a system (without losses) must be equal to the mass that leaves in the same time interval.

If the depth changed from an averaged depth of 0.5 m to 2 m, it means that the depth increased by 75%, so, a reduction of 70% for a maximum pick during syzygy results in a value that could be close to reality.

In Figure 35 shows an ebbing during spring tide, corresponding to the date 03-June. The colormap shows the depth averaged velocity differences between scenario one and two for flooding an ebbing during a spring tide, while the vectors are the change between both scenarios. There can be appreciated that the only area that presents an impact is the one corresponding to the dredging zone (local impact).

In the left, in red, it is marked the center of the polygon that was deepened, showing a decrease of 0.15 m/s, what agrees with the averaged results obtained for decreases during spring tides. The right figure shows that during flooding in spring tide, the decrease between both scenarios is smaller when compared with the ebbing, but impacts more areas around the deepened area.

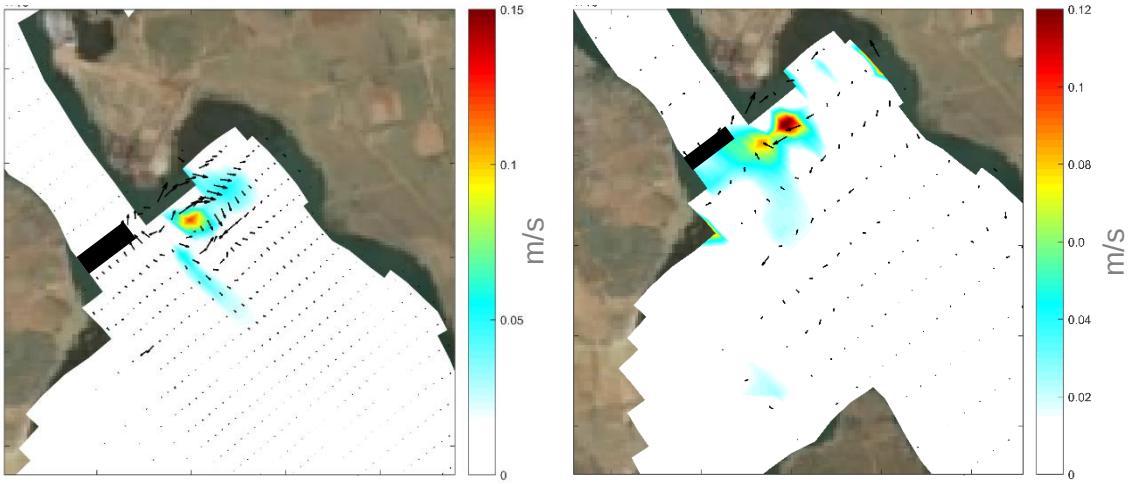

Figure 35. The left image corresponds to ebbing during spring tide and the image on the right corresponds to flooding during spring tide. Between the two images, there is a difference of 6 hours

From these figures, it's easier to appreciate that the higher changes appeared in ebbing during spring tides, but during flooding other areas around the deepened polygon showed a small decreased of the velocity to.

This map also shows an interesting behavior in the dredging area, where the vectors represents the difference in velocities between both scenarios, not the flow behavior. There is a greater difference in the area surrounding the dredging polygon, where the largest vectors are located. It is evident that the left figure, referring to the ebbing, presents the largest vectors while the right figure, corresponding to flooding, has smaller vectors.

The main problem that can be identified from the reduction in velocities is the possible accumulation of sediments in the area surrounding the deepened polygon. This area has the characteristic of being shallow and presenting large areas of seagrass, which can lead to accumulation of sediment in the surroundings.

A decrease in currents for such a shallow water body can represent future problems of sediment transport and erosion: the changes could promote deposition in the inner bay due to the lower current velocities.

The obtained results are similar with those obtained by (RENTERIA; CHIRINO,

2019), who studied the effects of dredging on the residence times of the water in Buenaventura Bay, Colombia, using a 2D finite elements hydrodynamic model coupled with a particle tracking model. The results of the comparison of the simulated scenarios, showed an important reduction in the velocities fields that allow an increase of the residence time up to 12 days in some areas of the bay.

6. CONCLUSIONS

A two-dimensional hydrodynamic model was applied to the San Quintín Bay coastal lagoon (SQBL). The hydrodynamic model was evaluated for sensitivity between astronomical tide and meteorological tide, and subsequently validated with the time series for currents and water level. The model satisfactorily represented both sea level and velocities, obtaining large correlation coefficients and low values for errors (MAE and RMSE). The model results showed that is capable of reproduce the essential hydrodynamics in the San Quintin Bay Lagoon, and can be forced by the astronomical tide and wind.

The results of the simulations carried out, to assess the sensitivity of the hydrodynamic model, indicate that the forcement with the greatest influence on the elevations and currents in San Quintin Bay Lagoon is the astronomical tide.

This model was used to create an understanding of the hydrodynamic changes that can be generated in the lagoon after deepening (by dredging activity) in a small area in the east arm, for which two scenarios were simulated: the current scenario without modified bathymetry and the second scenario with modified bathymetry simulating a dredging activity. The increase in depth caused a decreased of the water level (tidal range) and a decreased in velocities to, mainly during spring tides.

The maximum reduction in the tidal range was registered during spring tides reaching a value of 0.57 m decreased for one exceptional pick, while during neap tides the change was imperceptible. In averaged, the decreased on the water level for the whole simulated period was 4 cm. The exceptional pick could be a problem of calibration since this result did not repeat. The results suggest that the deepening of the area results in a larger impact in a localized way, leading to a decrease of the flow velocity over the deepened region, both in flood and ebb currents and throughout the whole quadrature/ syzygy cycle. The biggest changes due to deepening by dredging activity appeared during spring tides, where the currents registered a decrease of 0.14 m/s. The maximum decrease in velocities was found during a spring tide with a reduction of approximately 70%.

The results for the second simulated scenario pointed that the impact of the east arm deepening on the flow velocities is only in the deepened area region for ebbing during spring tide, and during flooding some other near areas presented a small reduction in the velocities to, mainly the areas near a small dam that is located to the left of the deepened area. The deepening area resulted in a reduction in the magnitudes of the velocities for the hole simulated period, with maior impact during spring tides. Reduction in ebbing currents during spring tide indicates a high risk of sediment accumulation in the area around the deepened polygon.

Regarding elevation, the results suggest a much smaller impact. Therefore, the hydrodynamic changes suggested by the results have the potential to impact the transport patterns of substances such as pollutants and sediments in San Quintin Bay Lagoon.

A decrease in elevations and velocities can be translated into larger retention times and higher times for water renewal in the north of the eastern arm (BSQ), compromising water quality. As well as being an area surrounded by agriculture and exponential human growth, this area could be affected by decreasing its ability to disperse contaminants and increase the sedimentation rates.

With a few exceptions, the long-term impact of dredging on suspended sediment concentrations has received fairly limited attention in scientific literature, therefore, this model could be used as a basis for future investigations that involve sediment transportation, water quality and the effect of deepening in tidal asymmetry and residual currents. It is paramount to be able to predict the consequences and effectiveness of the alternatives as accurately as possible, thus incorporating this information into decision making.

The long-term morphological effects of dredging are fairly well known due to the relatively large amount of (historic) topographic data in heavily modified estuaries.

7. REFERENCES

ABBOTT, M. B.; PRICE, W. A. Coastal, Estuarial and Harbour Engineers Reference Book. [S.l.]: [s.n.], 1994.

ALCAZAR, L. Modelación de la dinámica biogeoquímica. Ensenada, México. 2008.

AYÓN, J. M. H. et al. Variabilidad del CO2 total durante eventos de surgencia en Bahía San Quintín, Baja California, México. Ensenada: INE; CICESE, 2007.

BAKUN, A.; NELSON, C. S. Climatology of upwealling related processes of Baja California. *Coop Oceanic Fish Invest. California*, p. 107-127. 1977.

BAPTISTELLI, S. C. Análise crítica da utilização de modelagem matemática na avaliação da dispersão de efluentes leves no litoral da Baixada Santista (Estado de São Paulo). São Paulo: [s.n.], 2008.

BORREGO, S.; BORREGO , J. Temporal and spatial variability of temperature in two coastal lagoons. California Cooperative Oceanic Fisheries Investigations , v. XXlll, p. 188-197, 1982.

CASIAN , J. A. R. Ictofauna de la Bahía de San Quintín, Baja California, México, y su costa adyacente. Ciencias Marinas, 1996. Disponivel em: <http://dx.doi.org/10.7773/cm.v22i4.875>.

CHANES, R. Z. *Simulacion Numérica 3D de la hidrodinámica de Bahía San Quintín y su influencia en la distribucion de Nitrato*. Orientador: Xavier Flores Vidal. 2016. 96 f. Tesis (Maestría en Ciencias) - Facultad de Ciencias Marinas, México, 2016.

IBAR, V. M. C. et al. Geochemistry of modern sediments from San Quintín coastal lagoon, Baja California: Implication for provenance. *Revista Mexicana de Ciencias Geológicas*, México, v. 26, p. 117-132, 1 mar. 2009.

DELEU, et al. Morphodynamic evolution of the kink of an offshore tidal sandbank: the Westhinder Bank (Southern North Sea). *Continental Shelf Research*, p. 1587-1610, October 2004.

GONZALEZ , O. D. et al. La profundidad e hidrodinámica como herramientas para la selección de espacios acuícolas en la zona costera. Ciencias Marinas, v. 36, p. 249-265, 2010.

GONZALEZ, O.D. et al. San Quintin Lagoon Hydrodynamics Case Study. *Water Resources Management and Modelling*, 2012.

DELTARES. Delft3D-FLOW, User Manual. [S.l.]. 2014.

DELTARES. Delft3D-FLOW: User mannual. Version: 3.15.34158. ed. [S.l.]: [s.n.], 2014.

DÍAZ, P. Determinación de la circulación en Bahía San Quintín B.C. por gradientes de densidad. UABC. Ensenada. 1980.

DORMAN, C. et al. World marine fog analysis based on 58-years of ship observations. *Internatio Journal of Climatology,* 2018.

ELKEN, J. Dynamical Oceanography. Tallinn University of Technology. [S.l.].

ENTRINGER, F. C. MODELAGEM DA QUALIDADE DA ÁGUA DA BAÍA DE VITÓRIA, ES. Vitoria: UFES, 2016.

FARRERAS , S. F. Hidrodinámica de Laguans Costeras. Ensenada: CICESE, 2006.

FERRARIN, C. et al. Hydraulic regime-based zonation scheme of the Curonian Lagoon. *Hydrobiologia*, v. 611, p. 133-146, 2008.

FIERRO C., J.; BRAVO R., M.; CASTILLO S., M. Characterization of the tidal regimeand currents along the channel moraleda (43O 54’ S - 45O 17’ S). *Ciencia y Tecnologia del Mar*, v. 23, 2000.

FISCHER, H. Mass transport mechanisms in partially stratified estuaries. *Journal of Fluid Mechanics*, v. 53, p. 671-687, 1972.

FITZPATRICK, J.; IMHOFF, J. Water Quality Models: A Survey and Assessment. Water Environment Research Foundation, 2001.

FLANDERS MARINE INSTITUTE. The Coastal Wiki, 2016. Disponivel em: <http://www.coastalwiki.org/wiki/Modelling_coastal_hydrodynamics>. Acesso em: 15 March 2019.

GANG JI, Z. Hydrodynamics and Water Quality. Modelling rivers, lakes and estuaries. New Jersey: John Wiley & Sons, Inc, 2008.

GARCIA , M. et al. Application of a three-dimensional hydrodynamic model for San Quintin Bay, B.C., Mexico. Validation and calibration using OpenDA. *Journal of Computational and Applied Mathematics,* p. 11, 2014. Disponivel em: <http://dx.doi.org/10.1016/j.cam.2014.05.003>.

GARRAT, J. R. Review of Drag Coefficients over Oceans and Continents. Division of Atmospheric Physics, Aspendale, Australia, 1977.

GERRISTEN, H. et al. Validation Document Delft3D-FLOW; A software system for 3D flow simulations. Deltares. 2007.

GERRISTEN, H. et al. Validation Document Delft3D-FLOW; A software system for 3D flow simulations. Delft. Deltares. 2007.

GOBBI, E. F. et al. Implementation of a water quality and hydrodynamic model for the Irai reservoir. *Brazilian Conference on Water Resources*, Curitiba, 2003.

GOMEZ, M. Aplicaciones de un modelo de dispersión en Bahía San Quintín, Baja California, México. 1980. 90 f. Centro de Investigación Científica y Educación Superior de Ensenada (M.Sc.) - UNAM, México, 1980.

HERNANDEZ, S. B. Análisis de procesos físico- biológicos acoplados en la Bahía de San Quintín, B.C., México. Ensenada: UABC, 2005. PHD

HOSACK, G. R. et al. Habitat associations of estuarine species: comparisons of intertidal mudflat, seagrass (Zostera marina), and oyster (Crassostrea gigas) habitats. *Estuarine Coastal and Shelf Science*, 2006.

IGLESIAS , G.; CARBALLO, R. Wave Energy Potencial Along the Dead Coast. Energy, v. 34, p. 1963- 1975, 2009.

KNOWLES, N.; CAYAN, D. R. Elevational Dependence of Projected Hydrologic Changes in the San Francisco Estuary and Watershed. *Climatic Change , Netherlands*, v. 62, p. 319- 336, 2004.

LACERDA, K. C. Modelagem hidrodinâmica e do transporte de sedimentos da Baía de Vitória, E.S.: impacto do aprofundamento do canal estuarino do Porto de Vitória. Vitoria: UFES, 2016.

LANKFORD, R. R. Coastal Lagoons in Mexico: their origin and classification. Estuarine Processes , New York, v. II, p. 182-215, 1976.

LARGE , W. G.; POND, S. Open ocean momentum flux measurements in moderate to strong winds. *Journal of Physical Oceanography*, v. 11, p. 324-481, 1981.

LARGIER, J. L. et al. WEST: A northern California study of the role of wind-driven transport in the productivity of coastal plankton communities. *Deep Sea Research Part I*I, v. 53, p. 2833–2849, 2006.

LARIOS, N. T. Hidrodinámica de la Bahía de San Quintín, B.C. Ensenada: UABC, 2006.

LESSER, G.R. et al. Development and validation of a three-dimensional morphological model. Coastal Engineering, Delft, v. 51, p. 883-915, 2004.

LEWIS, R.; ERFTEMEIJER, P. Environmental impacts of dredging on seagrasses: A review. Marine Pollution Bulletin, Delft, v. 52, p. 1553-1572, 2006.

LUCERO, I.V. Aplicación de un Modelo Numérico y Análisis de Condiciones Hidrodinámicas en Bahía de San Quintín, B.C. Ensenada: Centro de Estudios Superiores de Ensenada, 1979.

LUCERO, I.V.; MURO, C.H.R. Aplicación de un modelo numerico unidimensional a Bahía San Quintin, B. C. Ciencias MarinasMex), Ensenada, v. 7, 1977.

JUAREZ, T. V. Influencia de remolinos y procesos de mezcla en el intercambio de agua entre una laguna y el mar abierto, Bahía San Quintín, Baja California, México. Ensenada: [s.n.], 2014.

MAZCOSTA. Manejo Integral Costero, 2018. Disponivel em: <https://mazcosta.org/>. Acesso em: 6 March 2019.

MELAKU CANU, D. et al. Hydrodynamic properties of San Quintin Bay, Baja California: Merging models and observations. Marine Pollution Bulletin, p. 12, 2016.

MONREAL, M. A.; DE LEÓN , D.A. SALAS. Modelo unidimensional de corrientes en Bahía de San Quintín, B.C., México. Geofísica Internacional , México, v. 29, p. 249-257, 30 nov. 1990. Disponível em: http://www.revistas.unam.mx/index.php/geofisica/article/view/39441/35876. Acesso em: 21 ago. 2019.

OXAMENDI, J. I. M. Variabilidad de la circulación y sus causas en Bahía San Quintin, B.C. CICESE. Ensenada, Mexico. 1989. Masters

PENNEKAMP, J. G. S. et al. Turbidity Caused by Dredging; Viewed in Perspective. Terra et Aqua, v. 64, 1996.

PUGH, D. Tides, Surges and Mean Sea- Level. Great Britain: John Wiley & Sons Ltd., 1987.

RENTERIA , F. F.; CHIRINO , M. P. Effect of bathymetric changes on residence time in Buenaventura bay (Colombia). DYNA, Medellín, v. 86, 2019.

SERVICIOS TURISTICOS Y PESCA COMERCIAL LOS VOLCANES SPR DE RL. MANIFESTACIÓN DE IMPACTO AMBIENTAL: Construcción de un muelle acompañado de obras de apoyo como son; andadores de madera, explanada a

base de concreto, baños, estacionamientos, establecimiento de palapas y actividad de dragado, delegación de San Quintín,. Ensenada. 2014.

SIQUEIRA, J. Estudo do mecanismo de alagamento e secamento e modelo computancional 2D baseado em elementos finitos. Vitória: UFES, 2007.

SMITH, S. D. et al. Air-Sea Fluxes: 25 Years of Progress. Boundary-Layer Meteorology, v. 78, 1996.

SMITH, S.; BANKE, G. Variation of the sea surface drag coefficient with wind speed. *Quarterly Journal of the Royal Meteorological Society*, v. 101, p. 655-673, 1975.

STOMMEL, H.; FORMER, H. On the Nature of Estuarine Circulation. Wood Hole Oceanographic Institution. Massachussets, p. 84. 1952.

TOBÓN, C. A. P. Metodología para la validación de modelos hidrodinámicos utilizando amplia información de campo: aplicación a la Bahía Meldorf en la costa del Mar del Norte Alemán. Medellín: UNC, 2002.

TORRES, F. J. O. Anpalisis de mareas y predicción de velocidad mediante un modelo unidimensional en Bahía San Quintín, B.C. Ensenada: UABC, 1980.

VAN MAREN, D. S. et al. The impact of channel deepening and dredging on estuarine sediment concentration. *Continental Shelf Research*, v. 95, p. 1-14, 2015.

VAN RIJN, C. Principles of Sediment Transport in Rivers, Estuaries and Coastal Seas. University of Utrecht. Delt. 1993.

VARGAS, et al. Studies of flow pattern and pollutants dispersion of the south lagoon complex of Santa Catarina State, Brazil. XIV Brazilian Conference on Water Resources, 2003.

VIDAL, X. F. Circulación Residual en la Bahía de San Quintín, B.C. México. Ensenada: CICESE, 2006.

WILKS , D. S. Statistical Methods in the Atmospheric Sciences. International Geophysics Series, United States, v. 91, p. 627, 2006.

WILLMOT, C. J. Some Comments on the Evaluation of Model Performance. Bulletin of the American Meteorological Society, v. 63, p. 1309- 1313, 1982.

WINTERWERP, J. C. et al. Defining Eco-Morphodynamic Requirements for Rehabilitating Eroding Mangrove-Mud Coasts. Wetland , v. 33, p. 515-526, 2013.

ZARZUELO, C. et al. Estuarine,Coastal and Shelf Science, p. 1-11, 2015.